Cold Season Performance of the NU-WRF Regional Climate Model in the Great Lakes Region

MICHAEL NOTARO,[a] YAFANG ZHONG,[b] PENGFEI XUE,[c] CHRISTA PETERS-LIDARD,[d] CARLOS CRUZ,[e] ERIC KEMP,[e] DAVID KRISTOVICH,[f] MARK KULIE,[g] JUNMING WANG,[f] CHENFU HUANG,[c] AND STEPHEN J. VAVRUS[a]

[a] *Nelson Institute Center for Climatic Research, University of Wisconsin–Madison, Madison, Wisconsin*
[b] *Space Science and Engineering Center, University of Wisconsin–Madison, Madison, Wisconsin*
[c] *Department of Civil, Environmental, and Geospatial Engineering, Michigan Technological University, Houghton, Michigan*
[d] *Hydrosphere, Biosphere, and Geophysics Earth Science Division, NASA Goddard Space Flight Center, Greenbelt, Maryland*
[e] *NASA Goddard Space Flight Center, Greenbelt, Maryland*
[f] *Illinois State Water Survey, University of Illinois at Urbana–Champaign, Champaign, Illinois*
[g] *NOAA/National Environmental Satellite, Data, and Information Service, Madison, Wisconsin*

(Manuscript received 19 February 2021, in final form 13 July 2021)

ABSTRACT: As Earth's largest collection of freshwater, the Laurentian Great Lakes have enormous ecological and socioeconomic value. Their basin has become a regional hotspot of climatic and limnological change, potentially threatening its vital natural resources. Consequentially, there is a need to assess the current state of climate models regarding their performance across the Great Lakes region and develop the next generation of high-resolution regional climate models to address complex limnological processes and lake–atmosphere interactions. In response to this need, the current paper focuses on the generation and analysis of a 20-member ensemble of 3-km National Aeronautics and Space Administration (NASA)-Unified Weather Research and Forecasting (NU-WRF) simulations for the 2014/15 cold season. The study aims to identify the model's strengths and weaknesses; optimal configuration for the region; and the impacts of different physics parameterizations, coupling to a 1D lake model, time-variant lake-surface temperatures, and spectral nudging. Several key biases are identified in the cold-season simulations for the Great Lakes region, including an atmospheric cold bias that is amplified by coupling to a 1D lake model but diminished by applying the Community Atmosphere Model radiation scheme and Morrison microphysics scheme; an excess precipitation bias; anomalously early initiation of fall lake turnover and subsequent cold lake bias; excessive and overly persistent lake ice cover; and insufficient evaporation over Lakes Superior and Huron. The research team is currently addressing these key limitations by coupling NU-WRF to a 3D lake model in support of the next generation of regional climate models for the critical Great Lakes Basin.

SIGNIFICANCE STATEMENT: Climate change poses a serious threat to the vital natural resources of the Laurentian Great Lakes region. Complex lake–atmosphere interactions and limnological processes are a challenge for regional climate models. To address the threat of climate change, there is a clear need to further evaluate and develop modeling tools for the Great Lakes Basin. Here, we evaluate the regional performance of the National Aeronautics and Space Administration's regional climate model at high spatial resolution in support of ongoing efforts to develop the next generation modeling tool for the Great Lakes region.

KEYWORDS: Inland seas/lakes; Climate variability; Climate models

1. Introduction

The Laurentian Great Lakes are the Earth's largest collection of freshwater and an invaluable resource to society and wildlife (Botts and Krushelnicki 1988). The Great Lakes megaregion is home to over 55 million people (Todorovich 2009). The lakes critically support the United States' and Canadian economies through impacts on shipping, drinking water, power production, manufacturing, fishing, and recreation (Vaccaro and Read 2011). The basin contains a rich diversity of fish, animals, and plants (Crossman and Cudmore 1998) and ecologically valuable wetlands.

The Great Lakes exert a prominent effect on regional climate due to their large thermal inertia, variability as a moisture source to the atmosphere, and contrasts in moisture, heat, friction, and radiation compared to adjacent land (Changnon and Jones 1972; Scott and Huff 1997; Chuang and Sousounis 2003; Notaro et al. 2013a). Heat and moisture fluxes destabilize and moisten the boundary layer during autumn–winter (Bates et al. 1993; Blanken et al. 2011). The lakes' relative warmth and resulting enhanced low-level convergence make the basin a preferred region of wintertime cyclogenesis (Petterssen and Calabrese 1959; Colucci 1976; Eichenlaub 1979). Lake-induced precipitation peaks during September–March when cloud cover and precipitation are enhanced downwind of the lakes (Niziol et al. 1995; Scott and Huff 1996; Kristovich and Laird 1998). Overlake turbulent fluxes and lake-effect precipitation are dampened by mid- to late winter (February–March) as ice cover becomes extensive (Niziol et al. 1995; Brown and Duguay 2010).

The Great Lakes region has experienced dramatic climatic and limnologic changes (Kling et al. 2003; Wuebbles and

Supplemental information related to this paper is available at the Journals Online website: https://doi.org/10.1175/JHM-D-21-0025.s1.

Corresponding author: Yafang Zhong, yafangzhong@wisc.edu

DOI: 10.1175/JHM-D-21-0025.1

© 2021 American Meteorological Society. For information regarding reuse of this content and general copyright information, consult the AMS Copyright Policy (www.ametsoc.org/PUBSReuseLicenses).

Brought to you by MIT LIBRARIES | Unauthenticated | Downloaded 09/22/21 12:14 PM UTC

Hayhoe 2004; Wuebbles et al. 2010; Sharma et al. 2018), including a regime shift in lake-surface temperature (LST) and ice cover (Van Cleave et al. 2014). During 1900–2010, annual air temperatures rose by 0.88°C in the Midwest United States (Kunkel et al. 2013; Schoof 2013; Pryor et al. 2014; Zobel et al. 2017, 2018). Due to mutual surface–atmosphere warming (Manabe and Wetherald 1967) and resulting earlier lake stratification, Lake Superior's surface water temperatures increased by 2.5°C during July–September of 1979–2006, exceeding the regional atmospheric warming rate (Austin and Colman 2007; Zhong et al. 2016; Ye et al. 2019). The lakes' ice cover declined by 71% during 1973–2010 due to the aforementioned mutual surface–atmosphere warming (Wang et al. 2012; Mason et al. 2016). Rising lake temperatures, ice cover reductions, and increased frequency of intense cyclones supported a long-term positive trend in lake-effect snowfall (Burnett et al. 2003; Ellis and Johnson 2004; Kunkel et al. 2009), which locally reversed over portions of the Great Lakes Basin in recent decades (Bard and Kristovich 2012; Hartnett et al. 2014; Suriano and Leathers 2017; Clark et al. 2020). Heavy precipitation events have become more frequent (Kunkel et al. 2003, 2012; Easterling et al. 2000; Winkler et al. 2012), with an invigorated hydrologic cycle generating extreme lake level variations (Gronewold et al. 2013).

Given the importance of lake–atmosphere interactions and pronounced climate change in the Great Lakes Basin, there is a need to generate, evaluate, and improve climate modeling for the region. Large lakes and their regional climate influence are poorly resolved in coarse global climate models (Mallard et al. 2014, 2015; Briley et al. 2017). The Great Lakes' representation across the Coupled Model Intercomparison Project global climate models varies broadly among land, wet soil, ocean, or inland lake grid cells, with the most advanced representation in the Coupled Model Intercomparison Project global climate models based on 1D lake models (none are coupled to 3D lake models) with inappropriate assumptions for deep lakes (Roeckner et al. 2003; Briley et al. 2017). One rudimentary regional climate modeling approach consists of extracting sea surface temperatures from the initial and lateral boundary conditions datasets over the Atlantic Ocean, Pacific Ocean, or Hudson Bay and applying those oceanic sea surface temperature values as LST boundary conditions for the Great Lakes (Mallard et al. 2015; Spero et al. 2016; Sharma et al. 2018). Such erroneous LSTs, retrieved from oceans rather than lakes, can negatively impact simulated pressure and air temperature regionwide (Spero et al. 2016). Alternatively, regional climate models that apply historical, remotely sensed or reanalysis-based LSTs, rather than a coupled lake model, neglect hydrodynamic feedbacks and are impractical tools for developing climate projections (Sharma et al. 2018).

Regional climate models have been employed in an array of Great Lakes studies. Zhong et al. (2012) demonstrated the ability of select regional climate models to capture the lakes' impacts on regional climate and outperform global climate models. The Regional Climate Model version 4, coupled to a 1D lake model, was applied to examine the lakes' influence on atmospheric circulation, stability, moisture, and temperature; highlight model skill in capturing variability and trends in air temperature, ice cover, and snowfall; elucidate the mechanisms behind recent lake warming; and formulate winter severity projections (Notaro et al. 2013a,b, 2014, 2015, 2016; Zhong et al. 2016). Applying the "Providing Regional Climates for Impacts Studies" regional climate model, Zhang et al. (2020) projected that wintertime precipitation in the Great Lakes Basin would increase during this century. The Weather Research and Forecasting (WRF; Skamarock et al. 2008) Model is a commonly used regional climate model for the Great Lakes Basin. According to Shi et al. (2010), the nested WRF Model with 1-km grid spacing accurately simulated snowfall and cloud patterns from Canadian snowstorms. Wright et al. (2013) revealed a close association between Great Lakes' ice cover distribution and resulting snowfall pattern in WRF and concluded that coarse models cannot capture local water–ice–atmosphere interactions that regulate snowband intensity and distribution. Insua-Costa and Miguez-Macho (2018) estimated that, during lake-effect snowstorms in November 2014, 30%–50% of WRF-simulated precipitation downwind of the lakes originated from lake evaporation, similar to those estimated from observed water and ice fluxes (e.g., Kristovich and Braham 1998) Applying nested WRF with 3-km grid spacing, Shi and Xue (2019) determined that resolving LST spatial variations enhances surface wind convergence, vertical motion, and lake-effect snowfall on the lee sides of the Great Lakes. The WRF-based findings of Sharma et al. (2019) included enhanced skill due to spectral nudging (Rockel et al. 2008; Wang and Kotamarthi 2013), better performance during winter than summer, and successfully simulated lake-effect precipitation at both 12- and 4-km grid spacing. Complex lake–atmosphere interactions and lake-effect snowfall morphology require high-resolution modeling (Notaro et al. 2013a,b, 2015; Wright et al. 2013; Briley et al. 2017; Xiao et al. 2018; Shi and Xue 2019). Future climate projections for the Great Lakes Basin were developed by Gula and Peltier (2012) and Peltier et al. (2018) using WRF either uncoupled or coupled to the Freshwater Lake Model (Mironov 2008). Peltier et al. (2018) identified a wintertime cold bias in WRF coupled to the Freshwater Lake Model across the Great Lakes Basin.

More advanced regional climate models typically represent the Great Lakes using 1D lake models, which incorporate coupled lake–atmosphere interactions and can generally capture the broad spatiotemporal patterns of LSTs and ice cover (Gula and Peltier 2012; Notaro et al. 2013b), but are characterized by serious limitations. These shortcomings for large lakes include the lack of dynamic lake circulation, explicit horizontal mixing, or ice motion; an oversimplified stratification process; assumed instantaneous mixing of instabilities; and deficient treatment of eddy diffusivity (Martynov et al. 2010; Stepanenko et al. 2010; Bennington et al. 2014; Mallard et al. 2014, 2015; Gu et al. 2015; Sharma et al. 2018). Such regional climate models, coupled to a 1D lake model, generate excessive ice cover due to the absence of horizontal mixing and ice movement (Bennington et al. 2010; Notaro et al. 2013b; Xiao et al. 2016). One-dimensional lake models commonly produce an anomalously early stratification and positive bias in summertime LST (Bennington et al. 2014). Charusombat et al. (2018) revealed that WRF coupled to a 1D lake model,

Brought to you by MIT LIBRARIES | Unauthenticated | Downloaded 09/22/21 12:14 PM UTC

adapted from the Community Land Model version 4.5 (Subin et al. 2012; Oleson et al. 2013), produces excessive sensible and latent heat fluxes, compared to Great Lakes Evaporation Network measurements, that can be largely resolved by modifying the roughness length scales. One common approach to reduce vertical temperature profile errors in 1D lake models is to artificially enhance the vertical eddy diffusivity of deep lakes to imitate the neglected dynamic circulation and vertical mixing processes (Subin et al. 2012; Bennington et al. 2014; Lofgren 2014; Gu et al. 2015; Mallard et al. 2015). Nonetheless, 1D lake models remain incapable of representing key dynamic and thermodynamic processes of deep lakes (Xiao et al. 2016; Xue et al. 2017). Continued progress is needed to interactively couple high-resolution regional climate models to 3D lake models in order to resolve shear instabilities, mixing episodes, Ekman suction, upwelling, downwelling, coastal currents and jets, seiches, and ice motion (Martynov et al. 2010; Bennington et al. 2010, 2014; Beletsky et al. 2012; Fujisaki et al. 2013), and minimize LST and ice cover biases (Notaro et al. 2013b; Xue et al. 2015, 2017; Sharma et al. 2018; Ye et al. 2019).

The authors developed an advanced Great Lakes Basin modeling tool, consisting of the NASA-Unified Weather Research and Forecasting (NU-WRF; Peters-Lidard et al. 2015) model, nested to 3-km grid spacing, interactively coupled to the Finite Volume Community Ocean Model (Chen et al. 2003) to represent 3D lake hydrodynamics. This tool will benefit subsequent assessments of historical and future climatic and limnological changes, representing variability and change in lake temperature, ice cover, and lake circulation, along with providing a high-resolution, convection-permitting depiction of precipitation extremes. In support of this development process, the current paper explores the cold season performance of the current NU-WRF version across the Great Lakes Basin, including the identification of regionally optimal schemes and the impacts of 1D lake model coupling, spectral nudging, and the choice of cumulus parameterization, microphysics, longwave and shortwave radiation, and planetary boundary layer and surface layer schemes. The authors present data and methods in section 2, results in section 3, and discussion and conclusions in section 4.

2. Data and methodology

a. Model description and experimental design

NU-WRF is a state-of-the-art observation-driven integrated modeling system that represents aerosol, cloud, precipitation, and land processes at satellite-resolved, convection-permitting scales. It was developed based on the National Center for Atmospheric Research Advanced Research WRF Model coupled with chemistry (WRF-Chem; Grell et al. 2005; Skamarock et al. 2008), with enhanced physics coupling and optimal use of NASA's satellite products. The WRF dynamical core is coupled to the Goddard Space Flight Center Land Information System (Kumar et al. 2006; Peters-Lidard et al. 2007, 2015) and Goddard Chemistry Aerosol Radiation and Transport model (Chin et al. 2000), while incorporating multiple NASA-based microphysics and radiation packages (Wu et al. 2016). NU-WRF simulations here apply the Noah Land Surface Model, which prognostically computes soil moisture and temperature, permits fractional snow cover, and incorporates freeze–thaw soil physics (Mitchell 2001).

The current NU-WRF version permits two crude treatments of large lakes. Either LSTs can be provided by skin surface temperatures from the boundary condition dataset, without including a lake model or two-way lake–atmosphere interactions, or the atmosphere can be two-way coupled to the 1D Lake, Ice, Snow, and Sediment Simulator (Subin et al. 2012) from the Community Land Model version 4.5 (Oleson et al. 2013) with modifications by Gu et al. (2015). This 1D mass and energy balance scheme applies 0–5 snow layers on top of lake ice, 10 water layers (5-cm depth for top layer), and 10 soil layers at the lake's bottom. This lake model initially generated reasonable LSTs for shallow Lake Erie but vast biases for deep Lake Superior due to an underestimated vertical heat transfer. However, by amplifying the eddy diffusion parameter, Gu et al. (2015) reduced these LST biases in an artificial manner that does not directly address the key 3D processes in deep lakes.

The performance of NU-WRF and optimal model configuration are explored for the Great Lakes region during a select cold season with active lake-effect snowfall. Twenty simulations (Table 1) are generated, including eight primary runs (''Nud'': with spectral nudging and temporally invariant November LSTs; ''NoNud'': without nudging and with temporally invariant LSTs that are fixed at the initial warm November state; ''NudVary'': with nudging and temporally varying LSTs; ''NoNudVary'': without nudging and with temporally varying LSTs; ''Nud1D'': with 1D lake model and uniform lake depths; ''Nud1Ddep'': with 1D lake model and spatially varying lake depths; ''MorrNoL'': without 1D lake model and with Morrison combination; ''MorrL'': with 1D lake model and Morrison combination) for November 2014–March 2015 and 12 supplemental runs for only February 2015 (when temperature biases are most pronounced) to limit computational costs. The vertical resolution is assigned to 61 levels. The one-way nested configuration consists of an outer domain with 15-km grid spacing and inner domain with 3-km grid spacing (Fig. 1). Initial and lateral boundary conditions are provided by either the Global Data Assimilation System 0-h analysis or European Centre for Medium-Range Weather Forecasts interim reanalysis. Lake treatment includes LSTs provided as boundary conditions based on Global Data Assimilation System skin surface temperatures; or generated by application of a 1D lake model either with uniform (50 m for all lakes) or spatially varying lake depths, the latter based on the Kourzeneva (2010) dataset. Some simulations include spectral nudging to the large-scale atmospheric fields (wind components, air temperature, and geopotential height above the planetary boundary layer and specific humidity at all levels) to an approximate 600-km wavelength, which is the wavelength specified in numerous prior studies (Ferraro et al. 2017; Iguchi et al. 2017; Lee et al. 2017; Loikith et al. 2018).

Applied cumulus parameterization options for the outer domain include the Kain–Fritsch (Kain and Fritsch 1990; Kain 2004) and modified Tiedtke (Tiedtke 1989; Zhang et al. 2011) schemes, with resolved, unparameterized convection in the inner domain. The thermal roughness length in the bulk

Brought to you by MIT LIBRARIES | Unauthenticated | Downloaded 09/22/21 12:14 PM UTC

TABLE 1. Summary of the configuration applied in 20 NU-WRF simulations, with the first eight runs (in italics) covering November 2014–March 2015 and the remaining runs covering only February 2015. Columns include the name of the simulation and options for lateral boundary conditions [Global Data Assimilation System (GDAS) or European Centre for Medium-Range Weather Forecasts (ECMWF) interim reanalysis (ERA-I)], lake physics (1D lake model turned on or off), spatially varying lake depths, activation of spectral nudging, cumulus parameterization in the outer domain [Kain–Fritsch (KF) or Modified Tiedtke (ModT)], thermal roughness length [default or vegetation-dependent scheme (vegdep)], microphysics [Thompson et al. graupel scheme version 3.1, Morrison 2-moment scheme, or Goddard 3-class ice scheme], longwave radiation scheme [Goddard, stand-along Rapid Radiative Transfer Model (RRTM), or Rapid Radiative Transfer Model for General Circulation Models (RRTMG)], shortwave radiation scheme [Goddard, RRTMG, or Community Atmosphere Model (CAM)], planetary boundary layer scheme [Yonsei University (YSU), Mellor–Yamada–Nakanishi–Niino Level 2.5 (MYNN2.5), or Mellor–Yamada–Janjić (MYJ)], surface layer scheme [old MM5, MYNN surface layer, Monin–Obukhov–Janjić (MOJ), or revised MM5 Monin–Obukhov], and activation of Noah Land Surface Model snow physics changes. Nud and NoNud apply persistent November 2014 lake surface temperatures throughout their entire simulations.

Run name	LBCs	sf_lake_physics	use_lake depth	grid_fdda	cu_physics	iz0tlnd	mp_physics	ra_lw_physics	ra_sw_physics	bl_pbl_physics	sf_sfclay_physics	ua_phys
Nud	GDAS	Off	NA	On	KF	Default	Thompson	RRTMG	RRTMG	YSU	Old MM5	Inactive
NoNud	GDAS	Off	NA	Off	KF	Default	Thompson	RRTMG	RRTMG	YSU	Old MM5	Inactive
NudVary	GDAS	Off	NA	On	KF	Default	Thompson	RRTMG	RRTMG	YSU	Old MM5	Inactive
NoNudVary	GDAS	Off	NA	Off	KF	Default	Thompson	RRTMG	RRTMG	YSU	Old MM5	Inactive
Nud1D	GDAS	On	Uniform	On	KF	Default	Thompson	RRTMG	RRTMG	YSU	Old MM5	Inactive
Nud1Ddep	GDAS	On	Varying	On	KF	Default	Thompson	RRTMG	RRTMG	YSU	Old MM5	Inactive
MorrNoL	GDAS	Off	Varying	On	KF	Default	Morrison	RRTM	CAM	MYNN2.5	MYNN	Inactive
MorrL	GDAS	On	Varying	On	KF	Default	Morrison	RRTM	CAM	MYNN2.5	MYNN	Inactive
MP3ICE	GDAS	On	Varying	On	KF	Default	Goddard	RRTMG	RRTMG	YSU	Old MM5	Inactive
PBLMYJ	GDAS	On	Varying	On	KF	Default	Thompson	RRTMG	RRTMG	MYJ	MOJ	Inactive
RAGODD	GDAS	On	Varying	On	KF	Default	Thompson	Goddard	Goddard	YSU	Old MM5	Inactive
SFCRMM5	GDAS	On	Varying	On	KF	Default	Thompson	RRTMG	RRTMG	YSU	Revised MM5	Inactive
MODTIED	GDAS	On	Varying	On	ModT	Default	Thompson	RRTMG	RRTMG	YSU	Old MM5	Inactive
ERAINT	ERA-I	On	Varying	On	KF	Default	Thompson	RRTMG	RRTMG	YSU	Old MM5	Inactive
UA_PHYS	GDAS	On	Varying	On	KF	Default	Thompson	RRTMG	RRTMG	YSU	Old MM5	Noah changes
IZ0TLND	GDAS	On	Varying	On	KF	veg-dep	Thompson	RRTMG	RRTMG	YSU	Old MM5	Inactive
RA_SWCAM	GDAS	On	Varying	On	KF	Default	Thompson	RRTMG	CAM	YSU	Old MM5	Inactive
MP_MORR	GDAS	On	Varying	On	KF	Default	Morrison	RRTMG	RRTMG	YSU	Old MM5	Inactive
SFC_MYNN	GDAS	On	Varying	On	KF	Default	Thompson	RRTMG	RRTMG	MYNN2.5	MYNN	Inactive
XUE_2DOM	GDAS	On	Varying	Off	KF	Default	Morrison	RRTM	CAM	MYNN2.5	MYNN	Inactive

Brought to you by MIT LIBRARIES | Unauthenticated | Downloaded 09/22/21 12:14 PM UTC

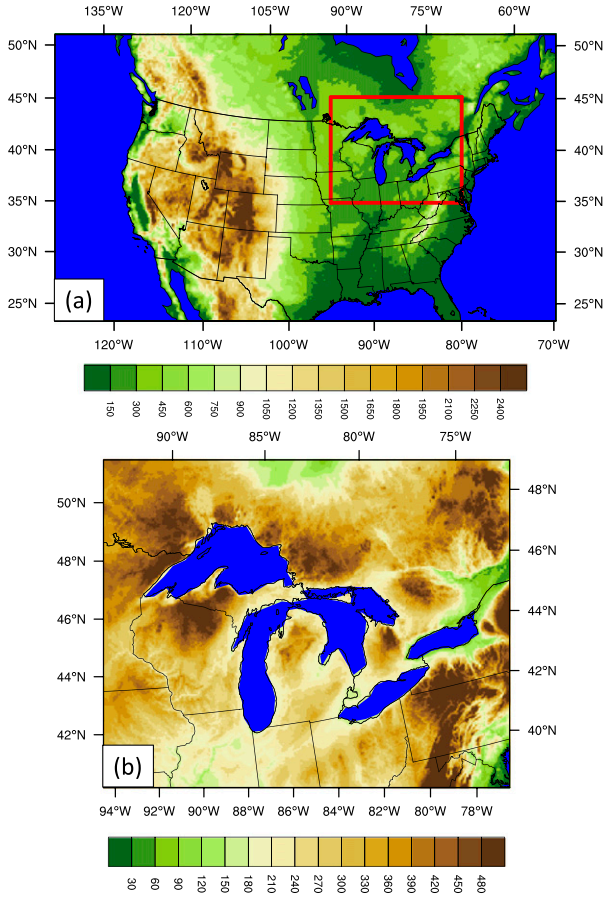

FIG. 1. Elevation maps (m) for the (a) outer domain with 15-km grid spacing and (b) inner domain with 3-km grid spacing.

transfer equations is either assigned to its default value or determined through a vegetation-dependent scheme (Chen and Zhang 2009; Weston et al. 2019). Applied microphysics options include the Goddard three-class ice scheme (Tao et al. 1989) and a couple of six-class, double-moment schemes, namely, the Thompson et al. (2008) graupel scheme and Morrison et al. (2009) scheme. Utilized longwave radiation schemes include the Rapid Radiative Transfer Model (RRTM; Mlawer et al. 1997), Rapid Radiative Transfer Model for General Circulation Models (RRTMG; Barker et al. 2007; Pincus et al. 2003), and Goddard scheme (Chou and Suarez 1999; Chou et al. 2001). The applied shortwave radiation schemes include the RRTMG (Iacono et al. 2008), Goddard (Chou and Suarez 1999; Chou et al. 2001), and Community Atmosphere Model (CAM; Collins et al. 2004) schemes. Applied planetary boundary layer schemes include the Yonsei University (Hong et al. 2006, 2010), Mellor–Yamada–Nakanishi–Niino Level 2.5 (MYNN2.5; Nakanishi and Niino 2006, 2009), and Mellor–Yamada–Janjić (MYJ; Mellor and Yamada 1982; Janjić 1990, 1994, 2001) schemes, and applied surface layer schemes include the Mesoscale Model Version Five (MM5) (Zhang and Anthes 1982), Mellor–Yamada–Nakanishi–Niino (MYNN; Nakanish 2001), Nakanishi and Niino, Monin–Obukhov–Janjić, and revised MM5 Monin–Obukhov (Jiménez et al. 2012) schemes. The UA_PHYS run activates improved physics of snowpack–vegetation canopy interactions, which increases sensible heat fluxes and decreases momentum roughness length over snowpack (Wang et al. 2010).

"Morrison combination" refers to the set of schemes applied in MorrL (with the 1D lake model) and MorrNoL (without the lake model), including Morrison microphysics, RRTM longwave radiation physics, CAM shortwave radiation physics, MYNN2.5 planetary boundary layer physics, and MYNN surface layer schemes. The improved simulations of air temperature and surface insolation due to the Morrison combination are primarily due to the Community Atmosphere Model's shortwave radiation scheme. The selection of the Community Atmosphere Model's shortwave radiation scheme is based on six test runs for December 2016–February 2017 varying, one by one, the microphysics scheme, shortwave radiation scheme, and boundary layer scheme (not shown). The Morrison combination is essentially the WRF configuration determined by Mooney et al. (2013) to produce the best simulated wintertime temperature simulation over Europe, who found that winter air temperatures are highly sensitive to the choice of radiation physics. Comparison of experiments reveals the regional impacts of spectral nudging, seasonally variant LSTs, 1D lake model coupling, spatially varying bathymetry, and Morrison combination. The effects of spectral nudging are isolated by [(Nud − NoNud) + (Nud_Vary − NoNud_Vary)]/2, of seasonally variant LSTs by [(Nud_Vary − Nud) + (NoNud_Vary − NoNud)]/2, of lake model coupling by [(Nud1D − Nud_Vary) + (Nud1Ddep − Nud_Vary) + (MorrL − MorrNoL)]/3, of spatially varying bathymetry by (Nud1Ddep − Nud1D), and of Morrison combination by [(MorrNoL − Nud_Vary) + (MorrL − Nud1Ddep)]/2.

b. Datasets

Three daily gridded observational datasets are used to evaluate model performance. First, the 1/8° North American Land Data Assimilation System version 2 (NLDAS-2) dataset (Xia et al. 2012) provides precipitation, surface pressure, 2-m specific humidity, 2-m air temperature, and 10-m zonal and meridional wind as primary forcings and surface albedo, sensible and latent heat fluxes, surface incident shortwave radiation, and liquid-equivalent snow depth as NLDAS-2 output from three land surface models (averaged here across models). The NLDAS-2 precipitation is derived through the temporal disaggregation of the gauge-only Climate Prediction Center analysis of daily precipitation (Higgins et al. 1996; Chen et al. 2008), performed on the NLDAS-2 grid with orographic adjustment; over Canada, only reanalysis precipitation is used due to poor gauge coverage, with the different data source applications across the United States–Canada border negatively impacting the performance of NLDAS-2 precipitation (Xu et al. 2019). NLDAS-2 surface downward shortwave radiation is computed by debiasing reanalysis with Geostationary Operational Environmental Satellite–based fields (Pinker et al. 2003).

Second, both directly measured and inferred variables are retrieved from the Oak Ridge National Laboratory's 1-km Daymet product (Thornton et al. 1997, 2014). These include

Brought to you by MIT LIBRARIES | Unauthenticated | Downloaded 09/22/21 12:14 PM UTC

precipitation and 2-m air temperature, as directly measured variables, and liquid-equivalent snow depth (based on a snow model) and 2-m vapor pressure (based on minimum temperature-dewpoint temperature relationships), as inferred variables. The relatively basic geographically weighted regression approach applied by Daymet, for interpolation from station observations to a gridded product, only accounts for elevation (Oyler et al. 2014).

Third, the 1-km National Weather Service's National Operational Hydrologic Remote Sensing Center Snow Data Assimilation System (SNODAS) dataset (Barrett 2003; Clow et al. 2012), which integrates data from satellite, airborne platforms, ground stations, and a snow model (Carroll et al. 2001), contains physical snow depth, liquid-equivalent snowfall, and liquid-equivalent snow depth. Several past studies (Hay et al. 2006; Azar et al. 2008; Clow et al. 2012) argued that SNODAS gridded snow water equivalent data had not been sufficiently evaluated, as SNODAS assimilates nearly all available ground-based and airborne observations of snow water equivalent, leaving insufficient independent data for evaluation.

While gridded observational datasets are valuable for model evaluation, they can exhibit intrinsic regional biases. Behnke et al. (2016) assessed multiple gridded observational datasets, compared to United States' station observations, and concluded that Daymet has the smallest temperature bias, NLDAS-2 has a warm bias and the greatest temperature bias, and Daymet has a wet bias and the greatest precipitation bias. These results justify the choice of Daymet for air temperature and NLDAS-2 for precipitation in the current paper's figures. King et al. (2020) identified a 50% positive bias in SNODAS snow water equivalent across Ontario compared to in situ observations, consistent with Zahmatkesh et al. (2019). Based on our comparison of snow water equivalent data from Daymet, NLDAS2, and SNODAS against these in situ observations, the current paper's figures focus on evaluating NU-WRF's snowpack against the more consistent NLDAS2 dataset.

Lakewide daily mean LST, derived from Advanced Very High Resolution Radiometer composite imagery (during cloud-free periods) but without inclusion of any buoy observations, is retrieved from the CoastWatch's Great Lakes Surface Environmental Analysis LST Dataset version 2, developed by NOAA's Great Lakes Environmental Research Laboratory (Schwab et al. 1992). Li et al. (2001) evaluated this CoastWatch LST satellite product against Great Lakes' buoy observations during May, July, and September of 1997 and concluded that mean differences were 0.26°C during the day and 1.52°C during the night. A year-round assessment by Schwab et al. (1999) found that the CoastWatch LSTs and buoy LSTs exhibited a mean difference of less than 0.5°C for all buoys and a root-mean-square difference (RMSD) ranging from 1.10° to 1.76°C. Persistent periods of cloud cover during the autumn–winter can restrict radiometer inputs to the Great Lakes Surface Environmental Analysis LST Dataset, degrading its reliability (Niziol 2003). New temperature imagery is not available over portions of the Great Lakes during the winter to early spring for as long as 30–50 days due to persistent cloud cover (Schwab et al. 1999). The lack of thermal imagery during spring and autumn is often most concerning, as lake temperatures often change rapidly during those seasons. As shown in Table S1, a comparison of the Great Lakes Surface Environmental Analysis Dataset with LST data at nine Great Lakes' buoys from the National Data Buoy Center during November 2014–March 2015 indicates the CoastWatch product has a mean bias of +0.93°C and RMSD of 1.63°C. The comparison is only based on an average of 37 days of data during the 2014/15 cold season as buoys are not deployed during much of the icy winter conditions. These findings are consistent with Niziol (2003), who concluded that during autumn, when lake temperatures are typically declining, the inability to update satellite-derived data due to persistent cloud cover can lead to a warm bias in the CoastWatch product.

Based on ice products from the United States National Ice Center and Canadian Ice Service, the Great Lakes Environmental Research Laboratory–Great Lakes Ice Cover Dataset contains lakewide daily mean ice cover (Assel et al. 2002, 2013; Assel 2005; Wang et al. 2012), although with the noted limitation that the dataset's spatial resolution, projection, and sampling frequency changed over time (Yang et al. 2020). Overlake measurements of air temperature, wind speed, downward shortwave radiation, sensible heat flux, and latent heat flux are obtained through the Great Lakes Evaporation Network (Blanken et al. 2011; Spence et al. 2011, 2013, 2019; Lenters et al. 2013) at Granite Island and Stannard Rock on Lake Superior, Spectacle Reef on Lake Huron, White Shoal on Lake Michigan, and Long Point on Lake Erie. The network's level 1 eddy covariance data have only undergone basic corrections, including removing sensible and latent heat spikes and a visual level of quality control. Moukomla and Blanken (2017) generated an independent dataset of Great Lakes' turbulent fluxes using the bulk aerodynamic approach, based on remote sensing, direct measurements, and reanalysis, and compared these modeled fluxes against GLEN observations, with the conclusion that they were in "good statistical agreement." The RMSD between the datasets at White Shoal, Stannard Rock, and Spectacle Reef lighthouses was 5.68, 6.93, and 4.67 W m^{-2}, respectively, for latent heat fluxes and 6.97, 4.39, and 4.90 W m^{-2}, respectively, for sensible heat fluxes.

3. Results

a. February 2015 performance among 20 simulations

To summarize NU-WRF's performance and identify the most successful model configuration for the Great Lakes region, four statistics are computed across the inner domain, namely, mean bias, RMSD, temporal correlation, and spatial correlation, based on daily 2-m air temperature, precipitation, snow water equivalent in the snowpack, surface incident shortwave radiation, and 2-m specific humidity for February 2015 among 20 simulations (Figs. 2 and 3).

1) AIR TEMPERATURE

A persistent atmospheric cold bias is evident in 18 runs and only absent in simulations with artificially constant November LSTs (Nud and NoNud, which do not permit the model to evolve beyond the initial warm November LST state) as

Brought to you by MIT LIBRARIES | Unauthenticated | Downloaded 09/22/21 12:14 PM UTC

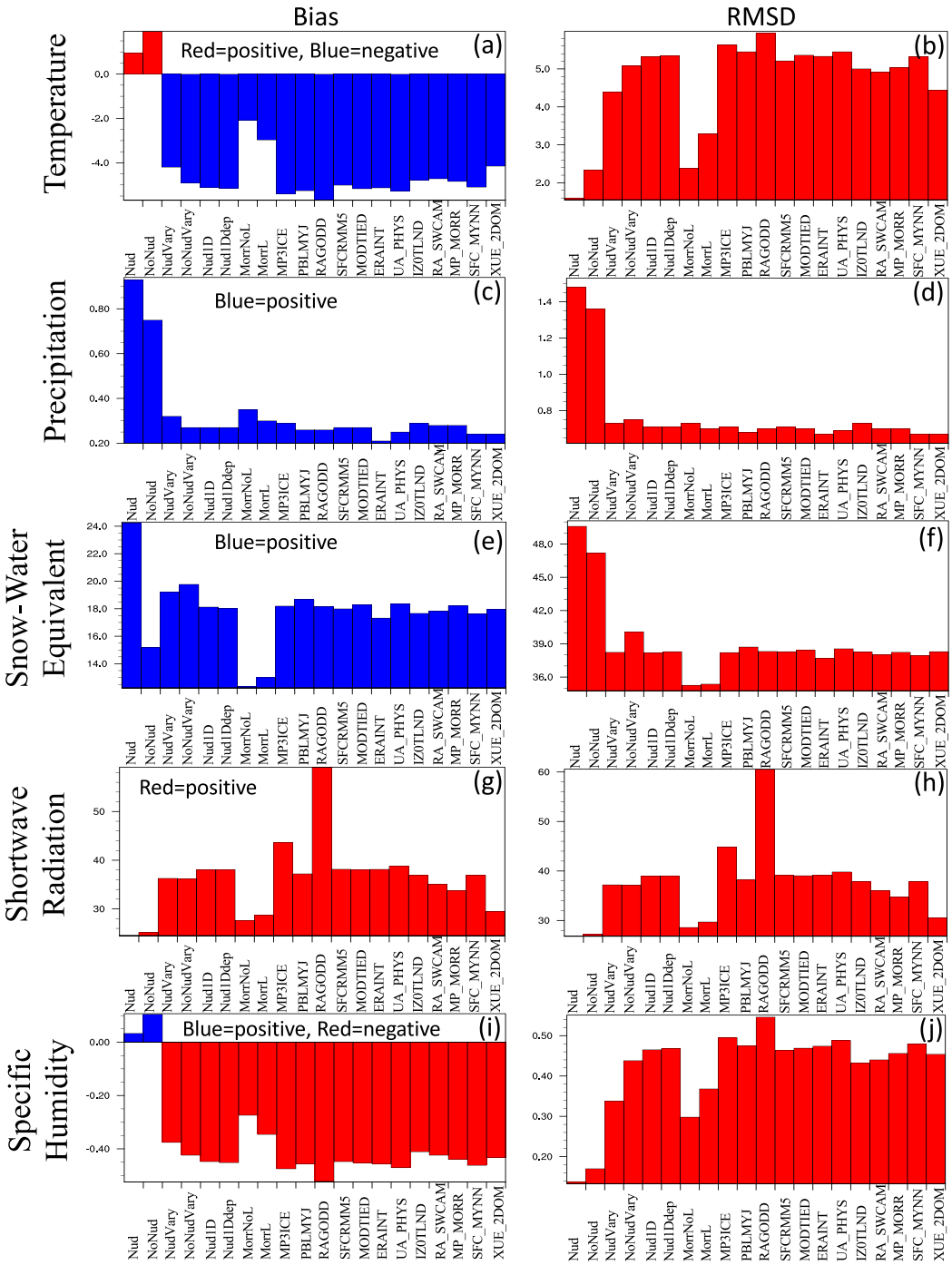

FIG. 2. (left) Bias and (right) root-mean-square difference in (a),(b) 2-m air temperature (°C), (c),(d) precipitation (mm day^{-1}), (e),(f) snowpack snow water equivalent (mm), (g),(h) downward surface shortwave radiation (W m^{-2}), and (i),(j) 2-m specific humidity (g kg^{-1}) across the Great Lakes region, over land, among 20 NU-WRF simulations for February 2015, compared to Daymet in (a) and (b) and NLDAS-2 in (c)–(j). Panels (g) and (h) closely match each other in magnitude, as all of the runs have a positive bias in solar radiation, which explains most of the RMSD.

unnaturally warm lakes maintain higher surrounding air temperatures (Fig. 2a). This is evidence of the lakes' basinwide influence on cold season climate. Among those 18 runs, the 2-m air temperature bias during February 2015 is least in MorrNoL (−2.09°C) and MorrL (−2.97°C), indicative of the Morrison combination dampening the regional cold bias, and greatest in RAGODD (−5.68°C), highlighting regional limitations of Goddard's radiation physics schemes. Lake model activation,

Brought to you by MIT LIBRARIES | Unauthenticated | Downloaded 09/22/21 12:14 PM UTC

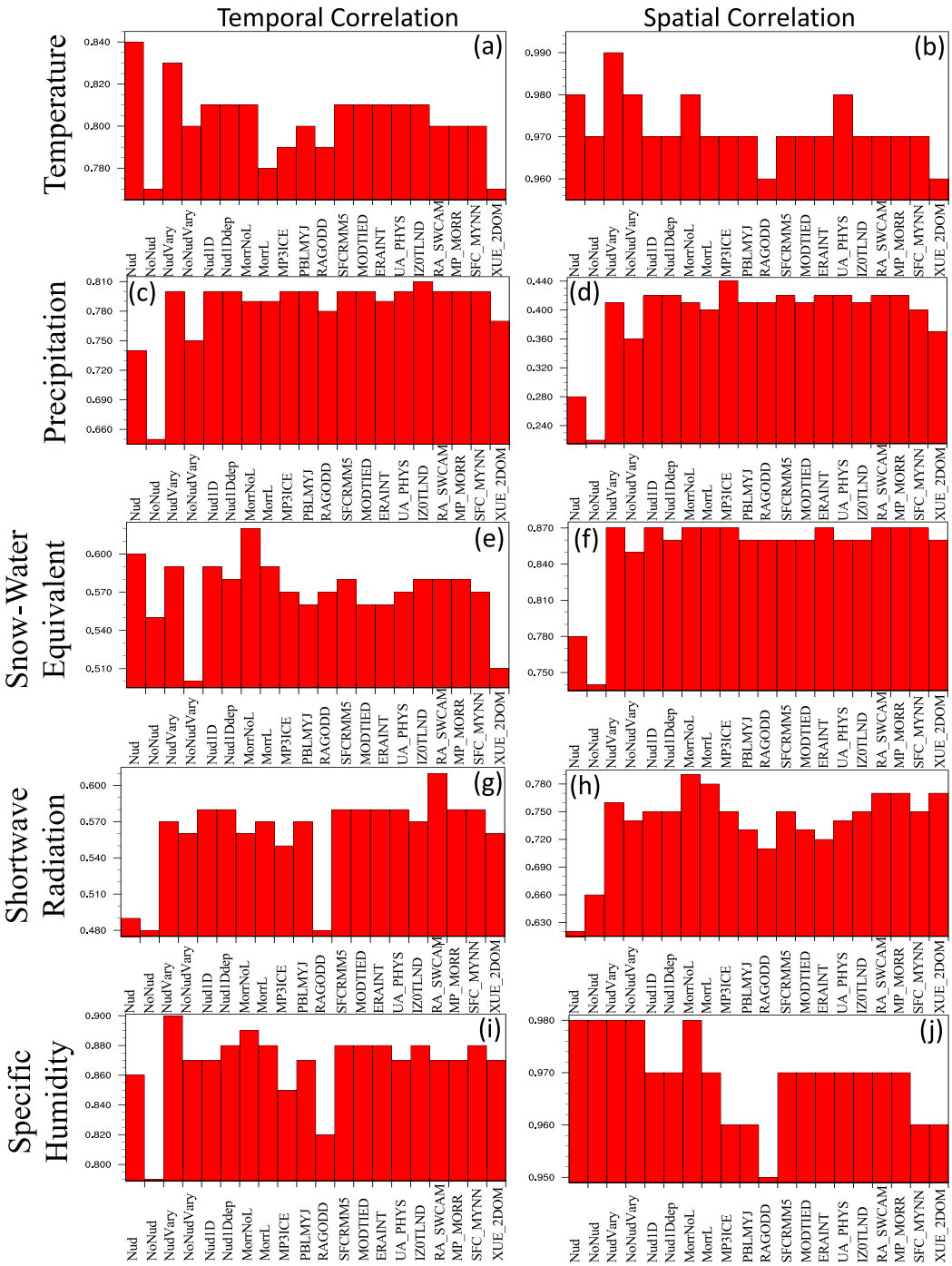

FIG. 3. (left) Temporal and (right) spatial correlations in (a),(b) 2-m air temperature, (c),(d) precipitation, (e),(f) snowpack snow water equivalent, (g),(h) downward surface shortwave radiation, and (i),(j) 2-m specific humidity across the Great Lakes region, over land, among 20 NUWRF simulations for February 2015, compared to Daymet in (a) and (b) and NLDAS-2 in (c)–(j). Correlation coefficients are saved to the hundredth decimal point, explaining why some runs appear to share the same exact correlation values.

while critical for representing lake–atmosphere interactions, enhances the cold bias (e.g., by 0.88°C from MorrNoL to MorrL). Based on RMSD, February air temperatures are best captured by Nud (1.60°C) and runs using the Morrison combination, namely, MorrNoL (2.38°C), and MorrL (3.29°C) (Fig. 2b). The seemingly good performance of Nud is deceiving, as unrealistically imposed November LSTs counter the intrinsic regional cold bias found in most of the simulations.

Brought to you by MIT LIBRARIES | Unauthenticated | Downloaded 09/22/21 12:14 PM UTC

The effects of individual model configuration choices on area-averaged 2-m air temperature over land in the inner domain during February 2015 are presented in Fig. S1 in the online supplemental material. For example, in order to isolate the typical magnitude of the effect of choice in microphysics scheme on simulated air temperatures, the Nud1Ddep, MP3ICE, and MP_MORR runs, which apply the Thompson, Goddard, and Morrison schemes, respectively, are compared against each other. Simulated February air temperatures in the inner domain are most sensitive to 1D lake model activation, spectral nudging, and choice of radiation and microphysics schemes. This further supports the conclusion that the benefits of the Morrison combination to air temperatures are primarily linked to the choice of radiation physics.

2) PRECIPITATION AND SNOWPACK

NU-WRF generates excessive overland precipitation during February 2015 among all simulations. This bias is vast for runs forced with November LSTs (e.g., Nud: $+0.95\,\mathrm{mm\,day^{-1}}$), as erroneously warm lakes support excessive lake-effect precipitation. The bias is moderate for runs with temporally varying LSTs, ranging from $+0.21\,\mathrm{mm\,day^{-1}}$ in ERAINT (using the European Centre for Medium-Range Weather Forecasts interim reanalysis for boundary conditions) and $+0.35\,\mathrm{mm\,day^{-1}}$ in MorrNoL (Fig. 2c). The precipitation RMSD ranges from $0.67\,\mathrm{mm\,day^{-1}}$ for ERAINT, SFC_MYNN, and XUE_2DOM to $1.48\,\mathrm{mm\,day^{-1}}$ for Nud (Fig. 2d). Compared to NLDAS2, all of the simulations produce excessive snow water equivalent in the snowpack, with the best results in MorrNoL (+12.3 mm) and MorrL (+13.0 mm) (Figs. 2e,f). Based on air temperature and precipitation statistics of bias, temporal correlation, spatial correlation, and RMSD among the lake model-enabled simulations (by tallying the frequency of a given run outperforming the remaining runs), the best performing runs during February 2015 are MorrL and XUE_2DOM, both applying the Morrison microphysics scheme, and worst are RAGODD and MP3ICE, which apply Goddard's radiation and ice microphysics schemes, respectively (Figs. 2 and 3).

The effects of individual configuration choices on area-averaged overland precipitation in the inner domain during February 2015 are shown in Fig. S2. Simulated February precipitation is most sensitive to the choice of lateral boundary conditions' dataset, spectral nudging, and 1D lake model activation.

3) SOLAR RADIATION

All of the runs generate excessive surface insolation in February 2015 (Fig. 2g), suggestive of insufficient cloud cover and atmospheric moisture, perhaps related to deficient lake evaporation or the atmospheric cold bias. As evidence, simulated mean precipitable water across the land within the inner domain is compared against the North American Regional Reanalysis (Mesinger et al. 2006) for February 2015, revealing negative biases of 5%–7% for the primary simulations of NudVary, NoNudVary, Nud1D, Nud1Ddep, MorrNoL, and MorrL (not shown). Insufficient atmospheric moisture supports exaggerated nighttime radiational cooling, leading, for example, in February to a 2-m daily minimum temperature bias of −4.5°C over land across the inner domain in Nud1Ddep, exceeding the cold bias of −2.8°C in 2-m daily maximum temperature. During the cold season, the mechanism of radiation cooling due to clear skies dominates over the warming effect of enhanced solar radiation during the season with short sunshine length. This finding is consistent with the study by Dai et al. (1999), which concluded for the study region that the greenhouse warming effect of clouds exceeds the solar cooling effect of clouds in winter. The Morrison combination supports smaller biases in surface insolation of $+27.6\,\mathrm{W\,m^{-2}}$ in MorrNoL and $+28.7\,\mathrm{W\,m^{-2}}$ in MorrL compared to the worst bias, $+59.1\,\mathrm{W\,m^{-2}}$ in RAGODD, thereby explaining the higher, more realistic air temperatures simulated with the Morrison combination. The model-versus-observed RMSD is lowest at $26.9\,\mathrm{W\,m^{-2}}$ for Nud, with artificially high LSTs enhancing evaporation, atmospheric moisture, and cloud cover; moderate when applying the Morrison combination (MorrNoL: $28.6\,\mathrm{W\,m^{-2}}$, MorrL: $29.7\,\mathrm{W\,m^{-2}}$); and highest for RAGODD at $60.5\,\mathrm{W\,m^{-2}}$ (Fig. 2h).

The effects of individual configuration choices on area-averaged overland incoming surface shortwave radiation in the inner domain during February 2015 are shown in Fig. S3. Simulated February insolation is most sensitive to the choice of radiation and microphysics scheme.

4) ATMOSPHERIC MOISTURE

Insufficient atmospheric moisture contributes to excessive incident solar radiation, as all of the runs, except for those forced by time-invariant November LSTs, exhibit negative biases in 2-m specific humidity during February 2015, ranging from $-0.27\,\mathrm{g\,kg^{-1}}$ in MorrNoL to $-0.52\,\mathrm{g\,kg^{-1}}$ in RAGODD (Fig. 2i). The Morrison combination reduces the humidity dry bias, with a relatively low RMSD of $0.30\,\mathrm{g\,kg^{-1}}$ in MorrNoL and $0.37\,\mathrm{g\,kg^{-1}}$ in MorrL. The bias and RMSD in 2-m specific humidity are lower in MorrNoL, without the lake model, than in MorrL, with the lake model. Activation of the 1D lake model leads to lower LSTs and excessive ice cover, which reduces lake evaporation in February across the deep lakes, Superior, Michigan, and Huron, leading to a regional decline in 2-m specific humidity and precipitable water. Goddard's radiation physics schemes in RAGODD generate lower model-versus-observed temporal correlations for specific humidity and shortwave radiation.

b. November 2014–March 2015 performance among eight simulations

Among the 20 simulations of February 2015, only eight are extended across November 2014–March 2015, namely, Nud, NoNud, Nud_Vary, NoNud_Vary, Nud1D, Nud1Ddep, MorrL, and MorrNoL. Analysis of these 5-month simulations permits a robust assessment of model performance and the impacts of spectral nudging, seasonally variant LSTs, 1D lake model coupling, spatially varying bathymetry, and Morrison combination. This Great Lakes regional assessment applies four statistical measures per month, namely, bias, temporal correlation, spatial correlation, and RMSD, between model output and overland observations (Tables S2–S5), focusing on 2-m air temperature, precipitation, snow water equivalent of the snowpack, surface incident shortwave radiation, and 2-m specific humidity (Fig. 4). The effects of spectral nudging are

Brought to you by MIT LIBRARIES | Unauthenticated | Downloaded 09/22/21 12:14 PM UTC

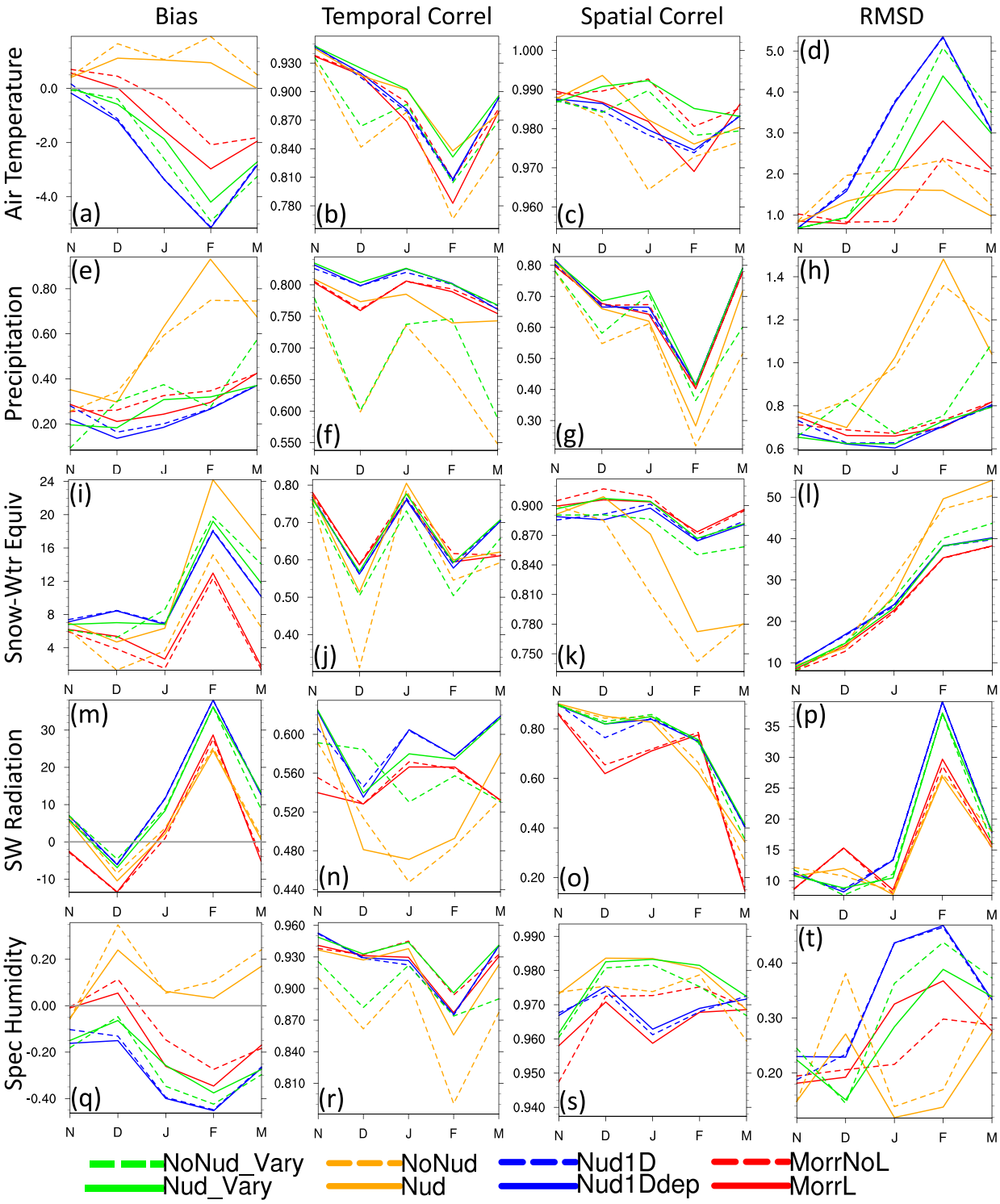

FIG. 4. (first column) Bias, (second column) temporal correlation, (third column) spatial correlation, and (fourth column) root-mean-square difference during November 2014–March 2015 in (a)–(d) 2-m air temperature (°C), (e)–(h) precipitation (mm day^{-1}), (i)–(l) snowpack snow water equivalent (mm), (m)–(p) surface downward shortwave radiation (W m^{-2}), and (q)–(t) 2-m specific humidity (g kg^{-1}) between observations [Daymet for (a)–(d) and NLDAS-2 for (e)–(t)] and eight NU-WRF simulations over land in the Great Lakes region.

Brought to you by MIT LIBRARIES | Unauthenticated | Downloaded 09/22/21 12:14 PM UTC

isolated by [(Nud − NoNud) + (Nud_Vary − NoNud_Vary)]/2, of seasonally variant LSTs by [(Nud_Vary − Nud) + (NoNud_Vary − NoNud)]/2, of lake model coupling by [(Nud1D − Nud_Vary) + (Nud1Ddep − Nud_Vary) + (MorrL − MorrNoL)]/3, of spatially varying bathymetry by (Nud1Ddep − Nud1D), and of Morrison combination by [(MorrNoL − Nud_Vary) + (MorrL − Nud1Ddep)]/2.

1) AIR TEMPERATURE

All of the runs, except for Nud and NoNud with time-invariant November LSTs, exhibit an atmospheric cold bias, most notably in February 2015 when the RMSD peaks (Figs. 4a,d). It is hypothesized that the extensive negative bias in daily minimum temperature during February is associated with excessive nighttime radiational cooling (given insufficient atmospheric moisture and clouds) and exaggerated inversion strength in the presence of the most extensive snowpack of the cold season. The Morrison combination substantially reduces this cold bias and associated air temperature RMSD (Figs. 4a,d). The November–March mean bias in 2-m air temperature, compared to Daymet, is reduced in magnitude from −2.55°C in Nud1Ddep to −1.18°C in MorrL, when comparing lake model-enabled runs, and from −1.87°C in NudVar to −0.64°C in MorrNoL, when comparing runs without the lake model, due to the use of the Morrison combination. The near-surface warming effect of the Morrison combination is most distinct over the Canadian portion of the inner domain and more pronounced at nighttime than daytime. Specifically, averaged across January–March 2015, the MorrL configuration compared to Nud1Ddep yields a mean increase in minimum 2-m air temperature of +2.1°C and in maximum 2-m air temperature of +0.9°C, thereby reducing the diurnal temperature range (not shown). By coupling NU-WRF to the 1D lake model, the atmospheric cold bias and air temperature RMSD increase due to poorly simulated LSTs and ice cover, and the temporal correlation between simulated and observed daily air temperatures declines (Figs. 4a–d). The November–March mean cold bias is amplified by 0.54°C between MorrNoL and MorrL, with the most notable cooling effect of the lake model close to the lakes and a comparable cooling impact on maximum and minimum 2-m air temperatures (not shown). Allowing LSTs to seasonally vary improves the temporal correlations for daily 2-m air temperature and is important for capturing daily variability in air temperature, precipitation, and insolation (Figs. 4b,f,j,n,r).

2) PRECIPITATION AND SNOWPACK

Simulated cold season precipitation is particularly sensitive to seasonally varying LSTs and nudging and less so to microphysics scheme and lake model coupling. Despite improved air temperatures, the Morrison combination modestly reduces the temporal correlations for precipitation (Fig. 4f) and physical snow depth (Table S3). Precipitation RMSD is mostly insensitive to lake model activation (Fig. 4h, e.g., MorrL versus MorrNoL). The constant LST simulations, Nud and NoNud, exhibit excessive January–March lake-effect precipitation and high precipitation RMSD (Figs. 4e,h), while time-variant LSTs in other simulations substantially improve these biases. Due to seasonally variant LSTs, the January–March wet precipitation bias, compared to NLDAS-2, is reduced from +0.64 mm day^{-1} in Nud to +0.33 mm day^{-1} in NudVary and from +0.70 mm day^{-1} in NoNud to +0.40 mm day^{-1} in NoNudVary (Fig. 4e). Nudging increases the spatial and temporal correlations and reduces precipitation RMSD, with increased temporal correlations for all analyzed fields, especially precipitation and physical snow depth (Fig. 4, Table S3). The mean temporal correlation across November–March for precipitation, compared to NLDAS-2, increases from 0.66 in NoNud to 0.77 in Nud and from 0.69 in NoNud_Vary to 0.81 in Nud_Vary, attributed to nudging (Fig. 4f). Based on temporal correlations, simulated daily precipitation exhibits greater consistency with the more accurate NLDAS-2 product (Fig. 4f) than Daymet (Table S3).

Compared to NLDAS-2, as the climatological snowpack becomes more extensive in mid- to late winter across the inner domain, simulated snow water equivalent exhibits a peak positive bias in February (Fig. 4i) and a peak RMSD in March (Fig. 4l). In fact, the mean error, defined as the absolute value of the bias, peaks in March, largely explained by the growing negative bias in snowpack water content across southern Canada that partly offsets the positive bias across much of the United States' portion of the inner domain. The low temporal correlation between observed and simulated daily snowpack snow water equivalent in February 2015 (Fig. 4j) is attributed to a regional mismatch over Wisconsin, Michigan, and southeastern Ontario, with an erroneous continued accumulation of snowpack in the model, given the simulated cold bias, when observations reveal that the snowpack was instead seasonally melting and retreating.

Several findings regarding simulated snow patterns are consistent across simulations, including model-versus-observed temporal correlations for daily liquid-equivalent snowfall, physical snow depth, and liquid-equivalent snow depth and spatial correlations for physical snow depth and liquid-equivalent snow depth compared to NLDAS-2 and SNODAS (Figs. 4j,k, Tables S3–S4), suggesting relatively lower sensitivity of these snow variables to experimental design. For example, the spatial correlation between simulated and SNODAS-observed daily physical snow depth ranges across experiments from 0.89 to 0.92 in November, from 0.82 to 0.89 in December, from 0.83 to 0.91 in January, from 0.82 to 0.88 in February, and from 0.83 to 0.89 in March (Table S4). The RMSD in physical snow depth and snow water equivalent of snowpack is comparable across the runs, as these variables are rather insensitive to model configuration (Table S5). Time-variant LSTs greatly reduce the snowfall RMSD (Table S5) and improve the temporal correlation for snow water equivalent downwind of Lake Superior. Nudging improves the spatial distribution of liquid-equivalent snowfall and snow depth and reduces snowfall RMSD (Tables S4 and S5). The model evaluation is limited by inconsistencies across observational datasets, especially for liquid-equivalent snow depth (Tables S2–S5).

3) SOLAR RADIATION AND ATMOSPHERIC MOISTURE

The most notable deficiencies in simulated surface insolation are a relatively high RMSD in February and low spatial correlation with observations in March (Figs. 4o,p). While the

Brought to you by MIT LIBRARIES | Unauthenticated | Downloaded 09/22/21 12:14 PM UTC

Morrison combination reduces the excess solar radiation bias and RMSD in January–March from $+20.8\,\mathrm{W\,m^{-2}}$ in Nud1Ddep to $+8.9\,\mathrm{W\,m^{-2}}$ in MorrL and reduces the specific humidity RMSD, it also weakens the temporal and spatial correlations in solar radiation (Figs. 4m–p,t). Temporal correlations for solar radiation and specific humidity are improved by seasonally varying LSTs (Figs. 4n,r).

To elucidate the cause of the atmospheric warming and reduced cold bias due to the application of the Morrison combination (specifically associated with the change in radiation physics packages), the surface energy budget components are computed, averaged over land across the inner domain, for the November–March simulations of Nud1Ddep and MorrL (not shown). The most pronounced mean seasonal changes due to the Morrison combination are an increase in surface downward longwave radiation of $+16.7\,\mathrm{W\,m^{-2}}$ (MorrL: $246.8\,\mathrm{W\,m^{-2}}$, Nud1Ddep: $230.1\,\mathrm{W\,m^{-2}}$) and decrease in surface downward shortwave radiation of $-10.5\,\mathrm{W\,m^{-2}}$ (MorrL: $97.5\,\mathrm{W\,m^{-2}}$, Nud1Ddep: $108.0\,\mathrm{W\,m^{-2}}$). This finding is consistent with an enhancement in atmospheric moisture and cloud cover with the Morrison combination.

4) Overall performance

Monthly statistics of bias, temporal correlation, spatial correlation, and RMSD are computed for an expanded set of 18 variables based on the eight runs for November 2014–March 2015 (Tables S2–S5). Technically, 14 variables (surface albedo, sensible heat flux, latent heat flux, precipitation, surface pressure, physical snow depth, liquid-equivalent snowfall, 2-m specific humidity, surface incident shortwave radiation, liquid-equivalent snow depth, 2-m air temperature, 10-m zonal wind, 10-m meridional wind, and 2-m vapor pressure) are assessed, although precipitation, liquid-equivalent snow depth, and 2-m air temperature are compared against 2–3 observational datasets each, leading to 18 total comparisons. For each simulation, 360 statistical values are computed, given four key statistics, 18 variables, and 5 months, and used to rank the models from 1 to 8. Based on the mean ranking, the best performing simulations are NudVary (with nudging and seasonally varying LSTs) and MorrNoL (with Morrison combination and nudging but no lake model) and worst are NoNud (without nudging, lake model, or seasonally varying LSTs) and NoNudVary (with seasonally varying LSTs but without nudging or lake model). It is striking that MorrNoL yields one of the best performances, while MorrL, with the conceptual advantage of including a simple lake model, only produces a moderate performance overall. When restricted to air temperature alone versus Daymet, the best performing runs are Nud, NudVary, and MorrNoL (all without the lake model) and worst are NoNud, Nud1D, and Nud1Ddep. When restricted to precipitation alone versus NLDAS-2, the best runs are Nud1Ddep, NudVary, and Nud1D and worst are NoNud, Nud, and NoNudVary.

Often, the simulated inner domain-averaged mean climate is not highly sensitive to modifications in the model configuration, as evident by comparing differences in biases between the better performing MorrNoL run and worse performing MorrL run in Tables S2–S5. More pronounced area-averaged differences between MorrNoL and MorrL due to lake model coupling, during November–March, include an 84% amplification in 2-m air temperature bias (versus Daymet) from -0.64°C in MorrNoL to -1.18°C in MorrL and a 69% amplification in 2-m specific humidity bias (versus NLDAS-2) from $-0.10\,\mathrm{g\,kg^{-1}}$ in MorrNoL to $-0.17\,\mathrm{g\,kg^{-1}}$ in MorrL. The RMSD in 2-m air temperature increases by 27% from 1.42°C in MorrNoL to 1.81°C in MorrL and in 2-m specific humidity increases by 12% from $0.24\,\mathrm{g\,kg^{-1}}$ in MorrNoL to $0.27\,\mathrm{g\,kg^{-1}}$ in MorrL. The most pronounced differences among simulations are noted when the analysis focuses on specific months and areas within the inner domain. For example, during January 2015, activation of the 1D lake model from MorrNoL to MorrL leads to 3°–6°C lower daily minimum temperatures across the Upper Peninsula of Michigan, reductions in precipitation of 20%–40% downwind of Lake Superior and 10%–30% downwind of Lake Huron, 50% increases in precipitation downwind of Lake Ontario, and 5%–20% enhancement in surface insulation across the state of Michigan (not shown).

Nudging improves spatial and temporal correlations and reduces the RMSD for many fields, such as by decreasing a simulated low-pressure bias over Canada and improving the temporal correlation for daily air pressure. NoNud generates poor temporal correlations given the lack of large-scale nudging. Often the highest temporal correlations are achieved by applying both nudging and Global Data Assimilation System-provided LSTs instead of the lake model. The Morrison combination improves the bias and RMSD of many fields, particularly by dampening the cold bias, but at the expense of weaker temporal correlations for multiple fields (Tables S2–S5). When activating the Morrison combination, performance statistics are generally improved for wind and air temperature (less drift from lateral boundary condition fields) but deteriorated for precipitation and physical snow depth (variables not present in the lateral boundary conditions).

5) Daily climate variability

The probability density functions of daily November–March 2-m air temperature and precipitation, averaged over land in the inner domain, are contrasted between the eight simulations and Daymet for temperature and NLDAS-2 for precipitation (Fig. 5). For the runs with seasonally varying LSTs (either with or without lake model coupling), the model generates too many very cold days with daily means below -20°C, especially in January–March (Figs. 5a,c); the biases are most pronounced on the cold side of the probability density function. Lake model coupling leads to too frequent very cold days below -20°C, as excessive ice cover restricts the lakes' wintertime warming influence on the atmosphere. The probability density function of daily mean air temperature is sensitive to the Morrison combination, which reduces the cold day frequency and increases the warm day frequency, and to temporally varying LSTs, which impose the opposite effect (Figs. 5a,c).

The model produces too few dry days and too many heavy precipitation days (Fig. 5b). The probability density function of daily precipitation is sensitive to the Morrison combination, which further deviates the probability density function from

Brought to you by MIT LIBRARIES | Unauthenticated | Downloaded 09/22/21 12:14 PM UTC

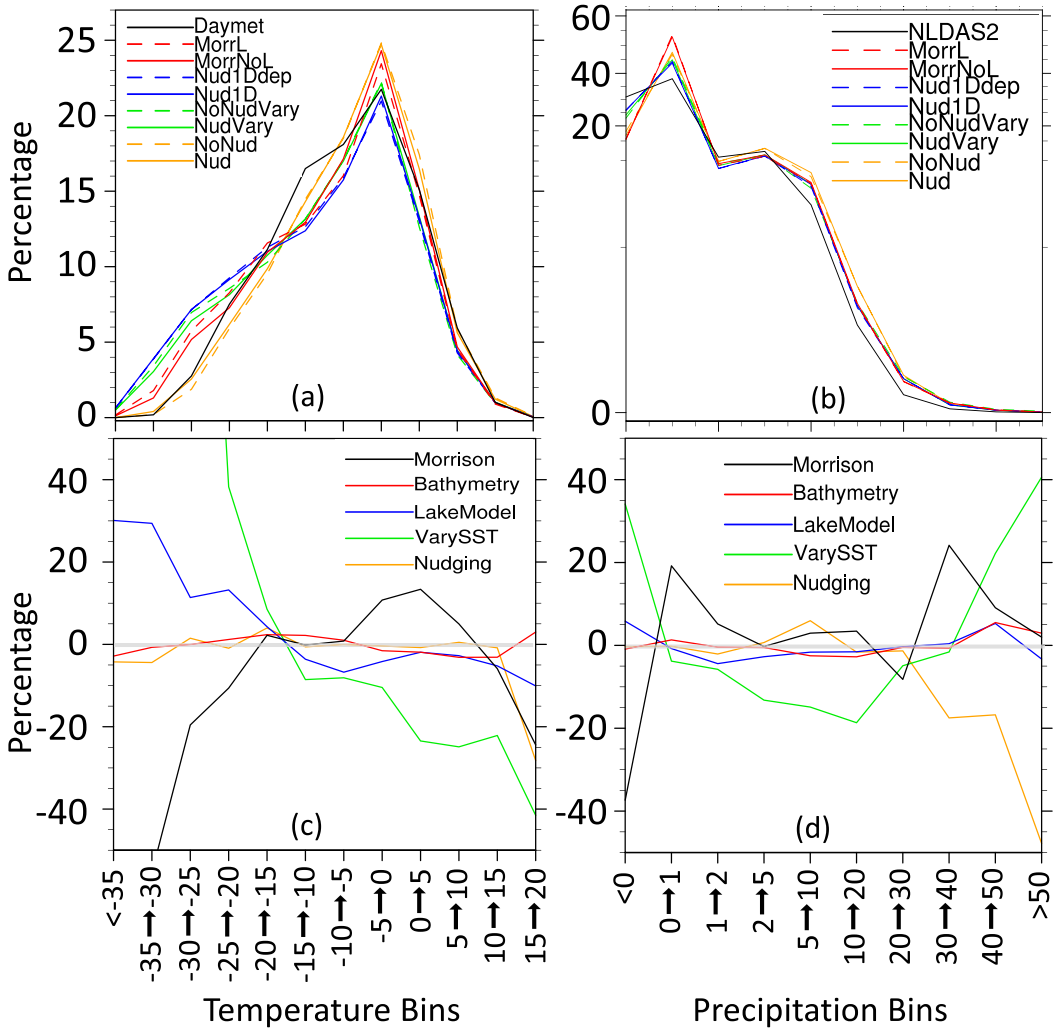

FIG. 5. Distribution of daily (a) 2-m air temperature (°C) and (b) precipitation (mm) in space and time across overland portions of the Great Lakes region inner domain, during November 2014–March 2015, according to bin values on the *x* axis. Data sources include NLDAS-2, Daymet, and eight NU-WRF simulations. Percentage change in the frequency of different bins of (c) air temperature and (d) precipitation values due to nudging, varying LST, 1D lake model implementation, spatially varying bathymetry, and Morrison combination.

observations by reducing the dry day frequency and increasing the days with drizzle, and to seasonally varying LSTs, which shift the probability density function closer to observations by increasing the dry day frequency and decreasing the number of days with drizzle (Figs. 5b,d). Nudging decreases the frequency of very wet days, more like observations (Figs. 5b,d).

c. *Spatial assessment of model performance and configuration impacts*

1) AIR TEMPERATURE

The discussion now shifts from an area-averaged assessment of model performance and the impacts of model configuration to a spatial assessment of simulated 2-m air temperature versus Daymet and simulated precipitation, liquid-equivalent snowpack, surface incident shortwave radiation, and 2-m specific humidity versus NLDAS-2 (Figs. 6–10). The model exhibits a regional cold bias during the cold season that is present as long as LSTs seasonally evolve beyond the relatively mild initial November state (Fig. 6). The air temperature bias is sensitive to time-variant LSTs, the Morrison combination, and lake model coupling and largely insensitive to spatially varying bathymetry and nudging (Figs. 6k–o). The Morrison combination substantially reduces the cold bias, holding it to below −2°C at most locations, although lake model activation somewhat dampens these benefits (Figs. 6i,j). The atmospheric cooling induced by the 1D lake model, and its LST and ice cover biases, is mostly confined to the basin (Fig. 6m), on the order of 0.5°–1.5°C, and coincides with atmospheric drying, enhanced pressure, and higher stability. The remaining areas of notable cold bias in excess of 2°C in MorrL (Fig. 6j) are downwind and in close proximity to the lakes and result from

Brought to you by MIT LIBRARIES | Unauthenticated | Downloaded 09/22/21 12:14 PM UTC

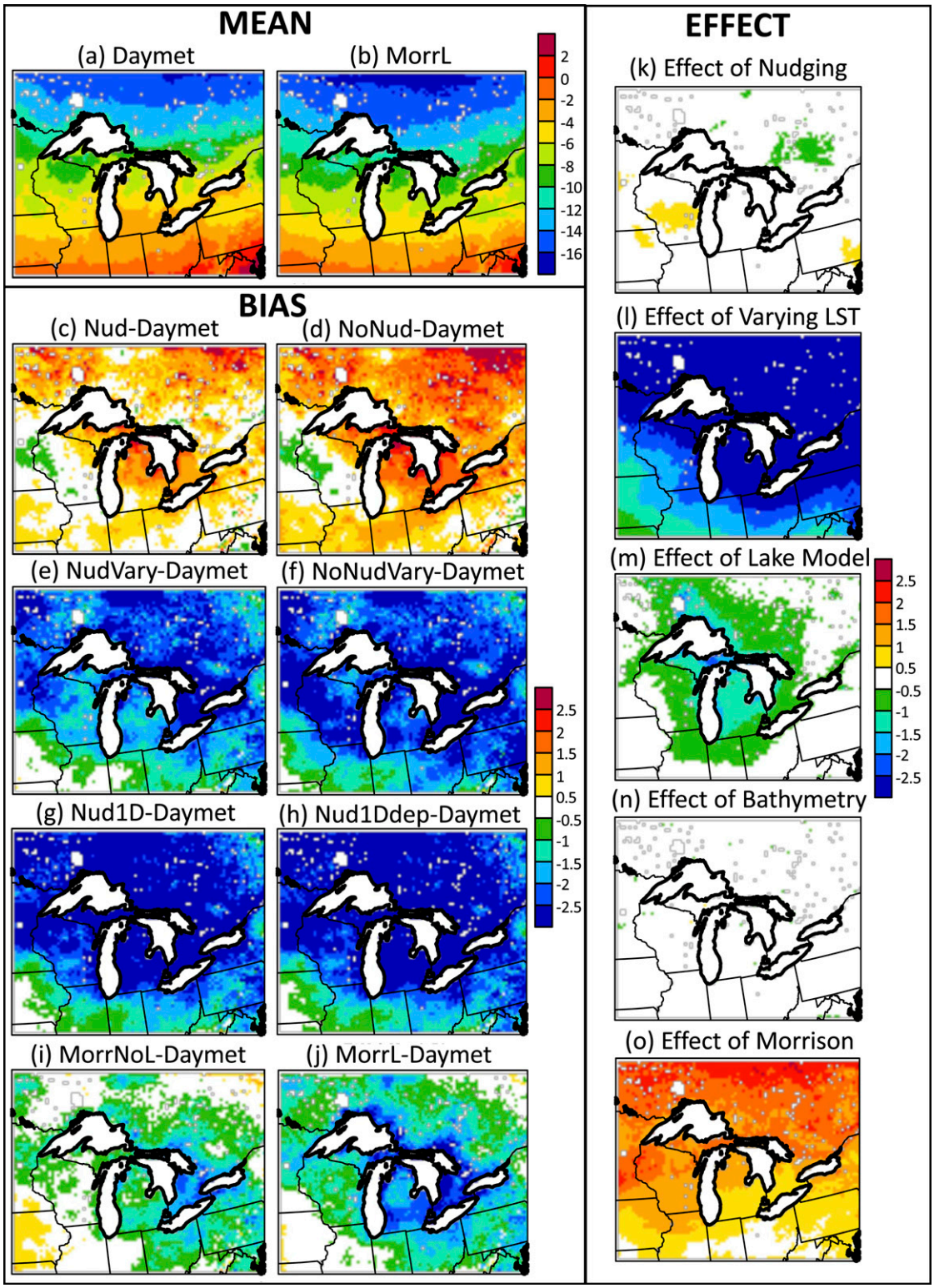

FIG. 6. Mean 2-m air temperature (°C) in (a) Daymet and the (b) MorrL run for November 2014–March 2015. Mean bias in 2-m air temperature (°C) during the same time period for the (c) Nud, (d) NoNud, (e) NudVary, (f) NoNudVary, (g) Nud1D, (h) Nud1Ddep, (i) MorrNoL, and (j) MorrL runs. Mean effect on 2-m air temperature (°C) during November 2014–March 2015 from (k) nudging, (l) varying LST, (m) 1D lake model implementation, (n) spatially varying bathymetry, and (o) Morrison combination.

Brought to you by MIT LIBRARIES | Unauthenticated | Downloaded 09/22/21 12:14 PM UTC

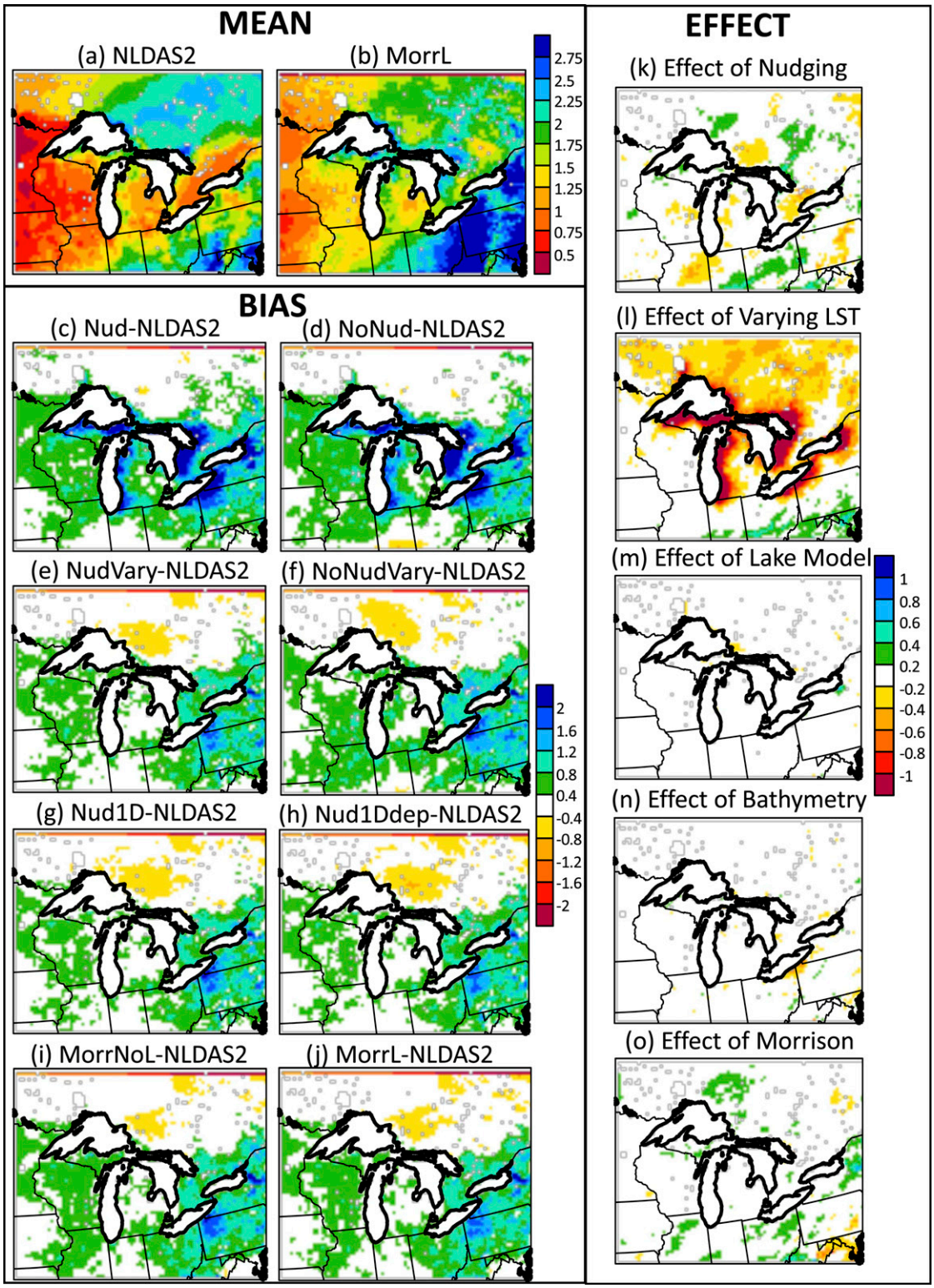

FIG. 7. Mean precipitation (mm day^{-1}) in (a) NLDAS2 and the (b) MorrL run for November 2014–March 2015. Mean bias in precipitation (mm day^{-1}) during the same time period for the (c) Nud, (d) NoNud, (e) NudVary, (f) NoNudVary, (g) Nud1D, (h) Nud1Ddep, (i) MorrNoL, and (j) MorrL runs. Mean effect on precipitation (mm day^{-1}) during November 2014–March 2015 from (k) nudging, (l) varying LST, (m) 1D lake model implementation, (n) spatially varying bathymetry, and (o) Morrison combination.

Brought to you by MIT LIBRARIES | Unauthenticated | Downloaded 09/22/21 12:14 PM UTC

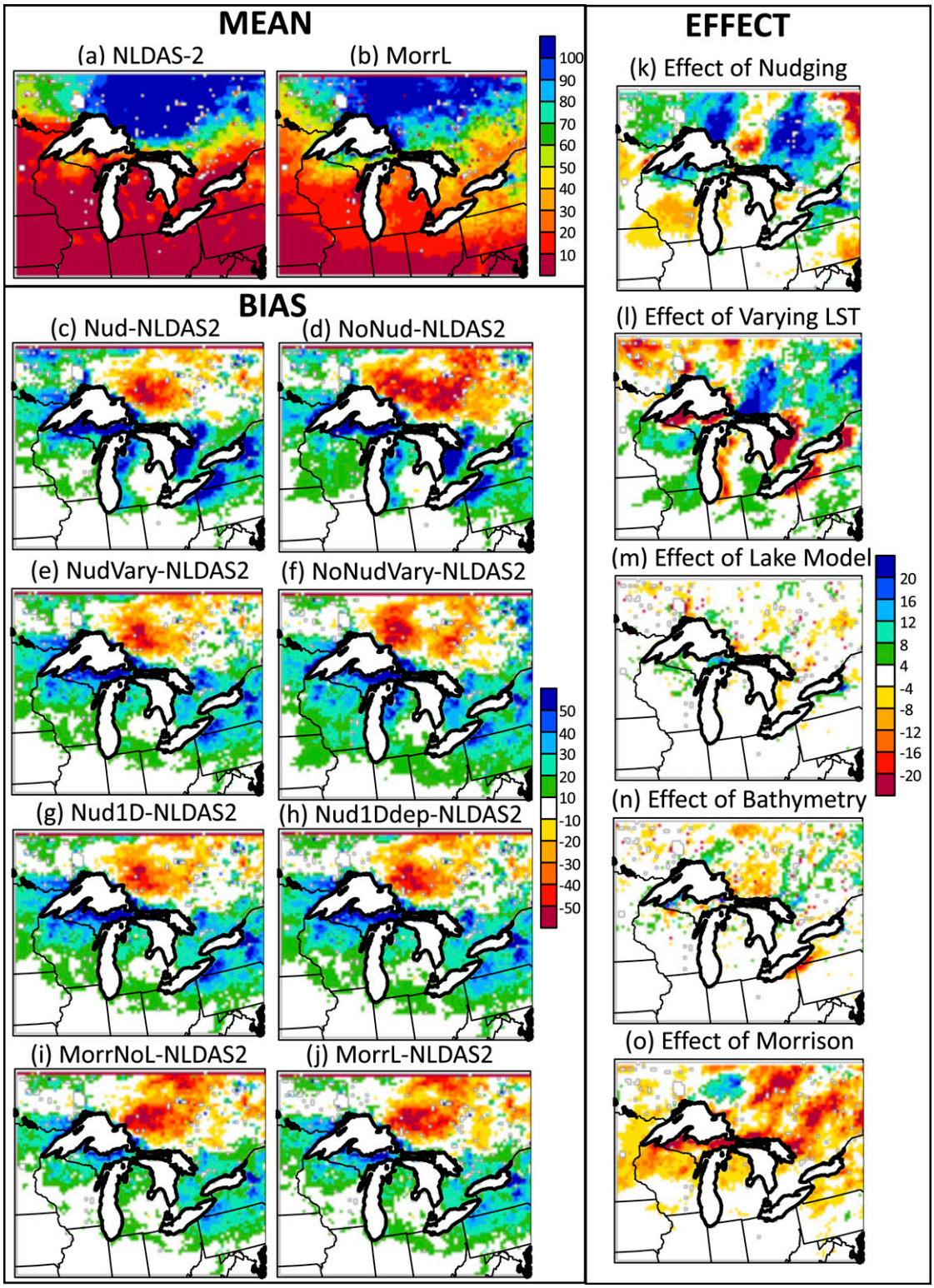

FIG. 8. Mean liquid-equivalent snowpack (mm) in (a) NLDAS-2 and the (b) MorrL run for November 2014–March 2015. Mean bias in liquid-equivalent snowpack (mm) during the same time period for the (c) Nud, (d) NoNud, (e) NudVary, (f) NoNudVary, (g) Nud1D, (h) Nud1Ddep, (i) MorrNoL, and (j) MorrL runs, Mean effect on liquid-equivalent snowpack (mm) during November 2014–March 2015 from (k) nudging, (l) varying LST, (m) 1D lake model implementation, (n) spatially varying bathymetry, and (o) Morrison combination.

Brought to you by MIT LIBRARIES | Unauthenticated | Downloaded 09/22/21 12:14 PM UTC

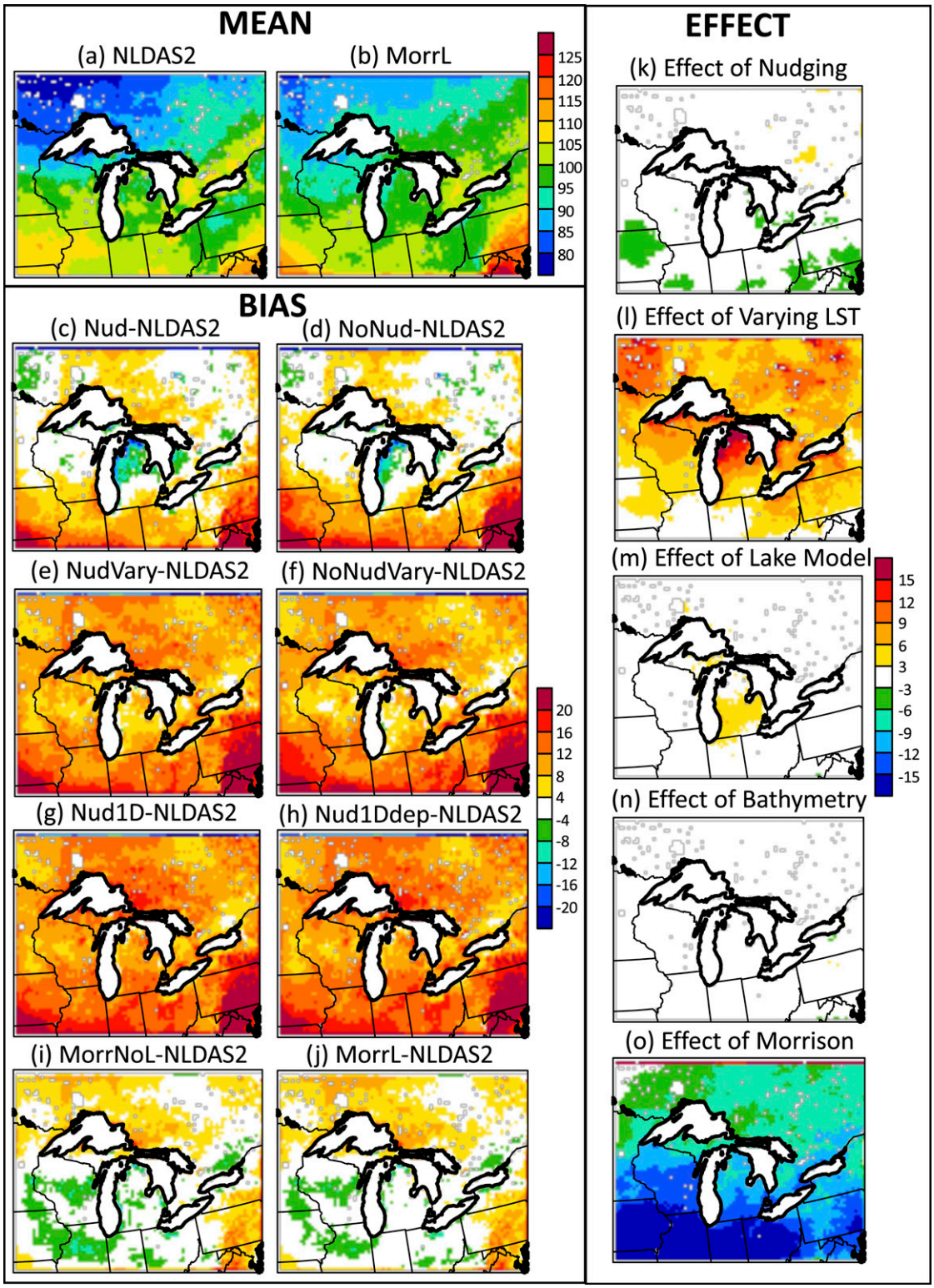

FIG. 9. Mean surface downward shortwave radiation (W m^{-1}) in (a) NLDAS2 and the (b) MorrL run for November 2014–March 2015. Mean bias in surface downward shortwave radiation (W m^{-1}) during the same time period for the (c) Nud, (d) NoNud, (e) NudVary, (f) NoNudVary, (g) Nud1D, (h) Nud1Ddep, (i) MorrNoL, and (j) MorrL runs. Mean effect on surface downward shortwave radiation (W m^{-1}) during November 2014–March 2015 from (k) nudging, (l) varying LST, (m) 1D lake model implementation, (n) spatially varying bathymetry, and (o) Morrison combination.

Brought to you by MIT LIBRARIES | Unauthenticated | Downloaded 09/22/21 12:14 PM UTC

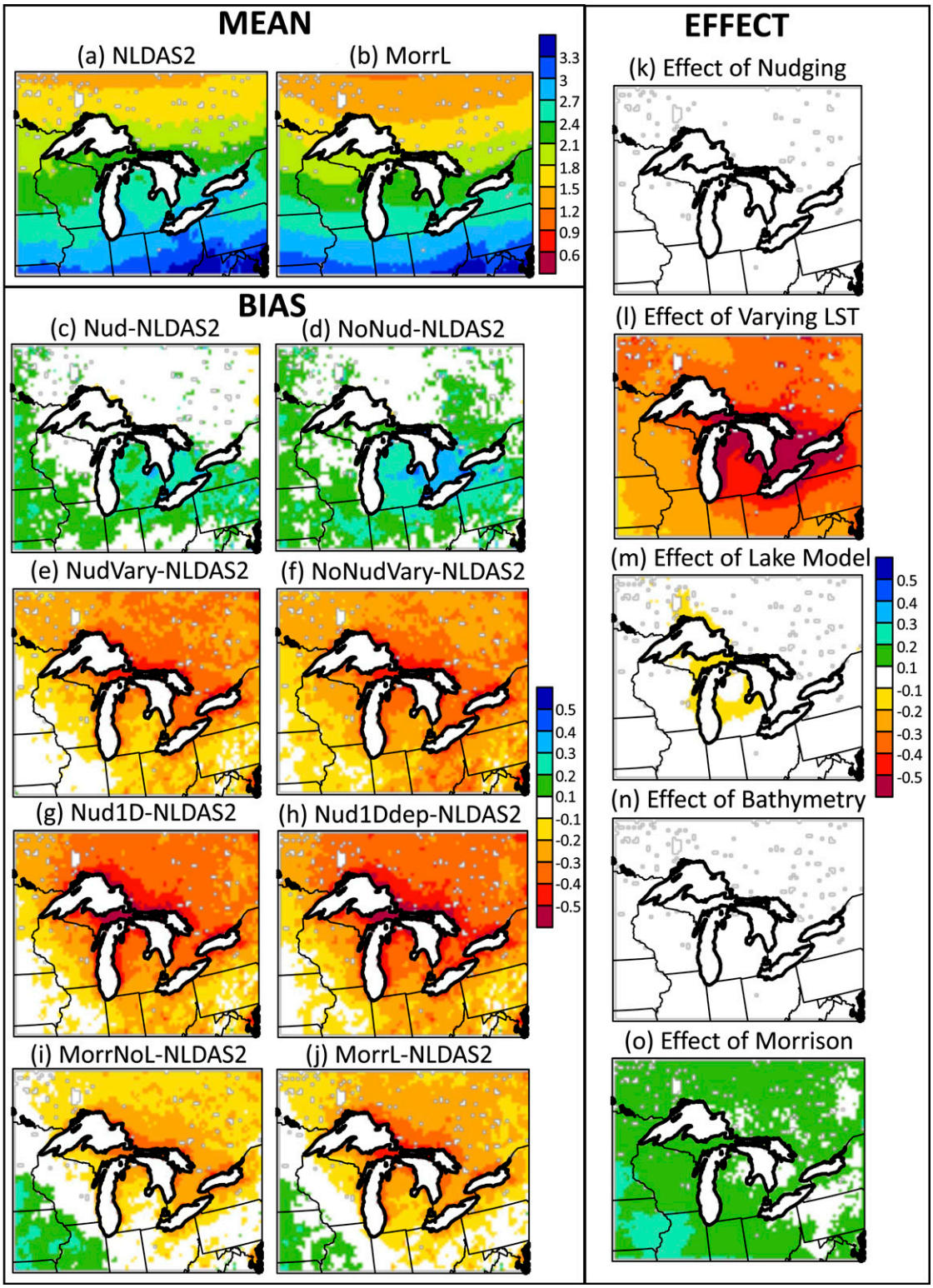

FIG. 10. Mean 2-m specific humidity ($g\,kg^{-1}$) in (a) NLDAS2 and the (b) MorrL run for November 2014–March 2015. Mean bias in 2-m specific humidity ($g\,kg^{-1}$) during the same time period for the (c) Nud, (d) NoNud, (e) NudVary, (f) NoNudVary, (g) Nud1D, (h) Nud1Ddep, (i) MorrNoL, and (j) MorrL runs. Mean effect on 2-m specific humidity ($g\,kg^{-1}$) during November 2014–March 2015 from (k) nudging, (l) varying LST, (m) 1D lake model implementation, (n) spatially varying bathymetry, and (o) Morrison combination.

Brought to you by MIT LIBRARIES | Unauthenticated | Downloaded 09/22/21 12:14 PM UTC

excessive ice cover and diminished heat fluxes from the lakes to the overlying atmosphere.

2) PRECIPITATION AND SNOWPACK

During November 2014–March 2015, the observed and simulated precipitation was lowest across Minnesota, Iowa, and Wisconsin and highest across Maryland, Virginia, West Virginia, and also central Ontario (Figs. 7a,b). Despite the consistency in the simulated versus observed spatial patterns of precipitation, all of the simulations produce excessive precipitation across the United States' portion of the inner domain, especially during January–March (Figs. 7c–j). The percent bias in MorrL precipitation is greatest over southeastern Ontario and Wisconsin. The fixed, artificially elevated LSTs (held fixed at the November values throughout the entire cold season simulation) in Nud and NoNud support excessive lake-effect precipitation (Figs. 7c,d,l). The Morrison combination slightly exaggerates the cold season wet bias (Fig. 7o). Nudging, lake model use, and heterogeneous bathymetry minimally impact the mean precipitation patterns (Figs. 7k,m,n). The near-shoreline features in Figs. 7 and 8 are not likely due to NLDAS-2's relatively coarse resolution as they are largely present in the higher resolution Daymet data.

Compared to NLDAS-2, the model generates excessive liquid-equivalent snow depth across much of the United States' portion of the inner domain but too little over central-southern Ontario (Figs. 8c–j), consistent with its precipitation biases (Figs. 7c–j). As evidence of this consistency, the spatial correlation between November–March mean biases in liquid-equivalent snow depth and precipitation across the inner domain in MorrL is 0.70 (N = 186 880 grid cells). The wet bias in precipitation is identified across 71% of the inner domain and in liquid-equivalent snow depth is identified across 76% of the inner domain, further supporting consistency between the variables' biases. The Morrison combination generally reduces the snow water equivalent, which improves the United States' biases but worsens biases over Ontario (Fig. 8o). We surmise systematic differences in lake-effect snowstorms between the Upper and Lower Great Lakes, with widespread broad coverage events dominating the former region versus single-band long lake axis parallel bands frequent in the latter region (Kristovich and Steve 1995; Rodriguez et al. 2007). Despite the lakes' pivotal role in regulating snowfall, lake model activation minimally impacts the spatial pattern and biases in liquid-equivalent snowpack (Fig. 8m). Seasonally varying LSTs permit more reasonable snowpack downwind of the lakes by reducing the excess bias in Nud and NoNud but favor excessive liquid-equivalent snow depth across much of the remaining inner domain (Fig. 8l). Nudging dramatically impacts liquid-equivalent snow depth across southern Canada, the Upper Midwest, and the Northeast, especially by reducing its negative bias across Ontario (Fig. 8k).

3) SOLAR RADIATION AND ATMOSPHERIC MOISTURE

Both NU-WRF and NLDAS-2 exhibit a northwest-to-southeast gradient in surface incident shortwave radiation during November 2014–March 2015 (Figs. 9a,b). Most of the simulations produce excessive solar radiation, although the Morrison combination substantially reduces this bias, especially across the United States' portion of the inner domain (Figs. 9i,j,o). Spatially varying bathymetry, lake model coupling, and nudging minimally impact this insolation bias (Figs. 9k,m,n). Temporally varying LSTs, beyond November's initial state, favor reduced cloud cover and atmospheric moisture and greater surface insolation (Fig. 9l).

Inconsistent with the positive precipitation bias, all of the runs with seasonally varying LSTs, whether applying a lake model or not, exhibit a cold-season dry bias in 2-m specific humidity (Figs. 10a–j), suggesting that the lakes are insufficient simulated sources of atmospheric moisture. The Morrison combination reduces the specific humidity dry bias (Fig. 10o). When applying persistent November LSTs, the artificially warm lakes in Nud and NoNud generate excessive evaporation and specific humidity (Fig. 10l). While the area-averaged November–March positive precipitation bias may seem inconsistent with the negative specific humidity bias and positive surface insolation bias (Fig. 4), spatial maps (Figs. 7, 9, and 10) reveal that the excessive precipitation, for example in MorrL, is mostly confined over the United States' portion of the inner domain while the deficient humidity and excessive solar radiation are mostly confined over southern Canada.

Simulated biases in precipitable water and surface insolation are broadly consistent during January–March, as evident by a spatial correlation of −0.69 across the inner domain in MorrL (not shown). Across the vast majority of the inner domain, especially downwind of the Great Lakes, insufficient precipitable water (at least partly linked to insufficient lake evaporation from overly icy lakes) leads to excessive surface insolation, with the exception isolated to the southwestern inner domain over Wisconsin, Minnesota, Iowa, and Illinois, where biases are positive for precipitable water and negative for solar insolation (now shown).

4) TEMPORAL CORRELATIONS

The model-versus-observed temporal correlation is computed by month during November 2014–March 2015, averaged across months, and plotted (Fig. 11) from MorrL for the following daily, overland variables: surface pressure, 10-m meridional wind, 10-m zonal wind, 2-m specific humidity, 2-m air temperature, snowpack water equivalent, snow depth, surface albedo, precipitation, surface incident shortwave radiation, sensible heat flux, and latent heat flux. These variables are generally listed in order of strongest to weakest correlations across the inner domain. For fields related to pressure, wind, specific humidity, and air temperature, which are among the variables provided through the lateral boundary conditions, temporal correlations exceed 0.8 for nearly the entire inner domain (Figs. 11a–e). In contrast, the model is less successful in reproducing the observed variability in surface insolation and turbulent fluxes (Figs. 11j–l). The precipitation temporal correlation is notably lower downwind of Lake Huron (Fig. 11i), although observational uncertainty is higher there due to limited station observations.

d. *Model assessment of LST and ice cover*

The LST time series during November 2014–March 2015 is assessed for the three extended runs that include a coupled 1D

Brought to you by MIT LIBRARIES | Unauthenticated | Downloaded 09/22/21 12:14 PM UTC

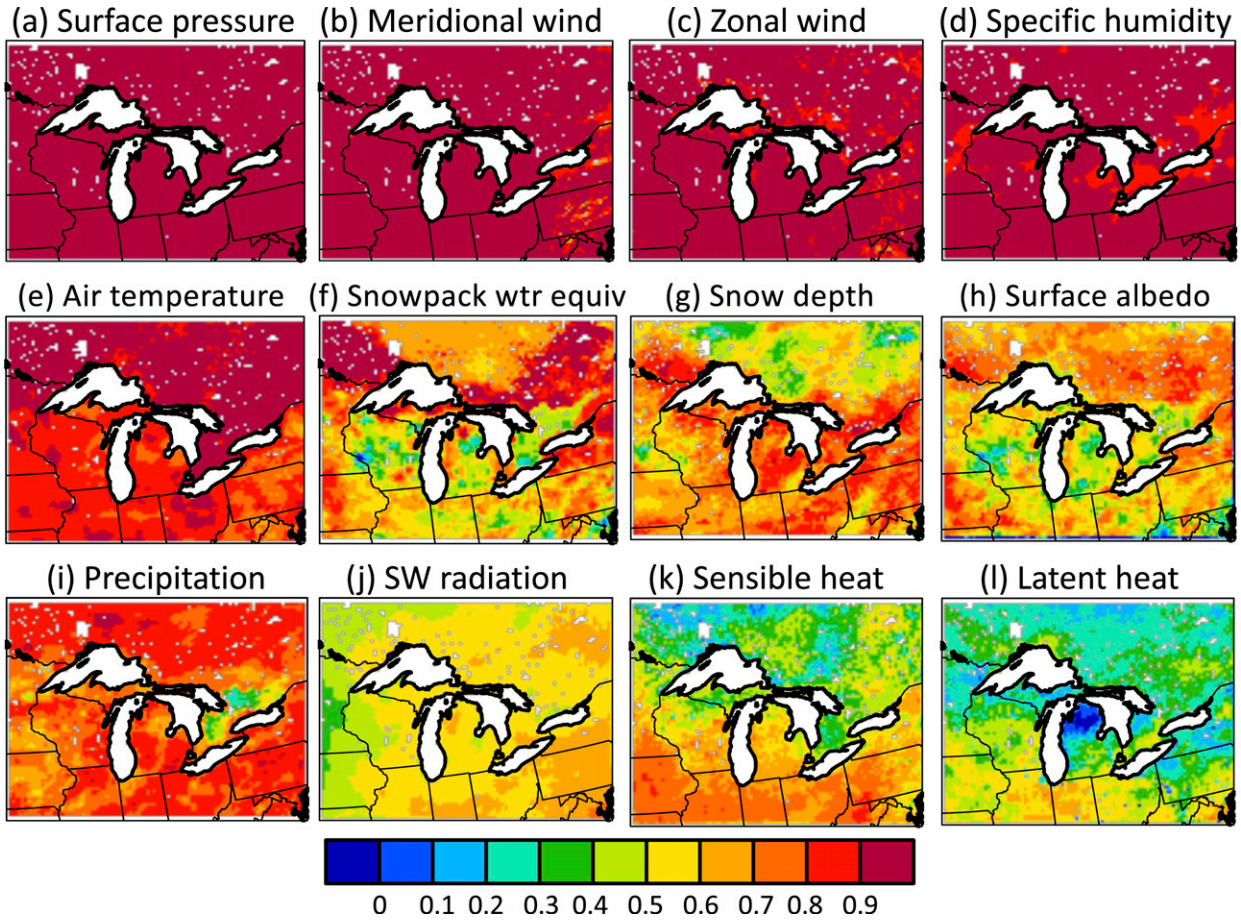

FIG. 11. Mean temporal correlation between MorrL-simulated and observed daily values of (a) surface pressure, (b) 10-m meridional wind component, (c) 10-m zonal wind component, (d) 2-m specific humidity, (e) 2-m air temperature, (f) snowpack snow water equivalent, (g) physical snow depth, (h) surface albedo, (i) precipitation, (j) surface downward shortwave radiation, (k) sensible heat flux, and (l) latent heat flux. One correlation is performed per calendar month during November 2014–March 2015, and then the average of the five correlations is plotted. The observational datasets include NLDAS2 for (a)–(d), (f), and (h)–(l), Daymet for (e), and SNODAS for (g). Plots are generally ordered by variable with the strongest to weakest correlations.

lake model, namely, Nud1D, Nud1Ddep, and MorrL, compared with the Great Lakes Surface Environmental Analysis (Fig. 12). All three runs produce cold LST biases across the five lakes, ranging from −0.8°C for Erie to −1.6°C for Michigan in Nud1D, from −1.4°C for Superior to −1.7°C for Michigan in Nud1Ddep, and from −1.2°C for Superior to −1.6°C for Michigan in MorrL (Fig. 12). LST biases for Superior are least in MorrL and for Erie are least in Nud1D. The simulated initiation of fall turnover (when LST drops to 4°C) occurs too early. The observed date ranges from 27 November for Superior to 6 January for Ontario, while the simulated date in MorrL occurs in November for all five lakes (Fig. 12). Some of this apparent simulated cold lake bias is explained by the inherent warm bias of the Great Lakes Surface Environmental Analysis product due to insufficient satellite retrievals during prolonged cloudy periods in the autumn–winter. The temporal correlation between observed and simulated LSTs is lowest for Superior, ranging from 0.80 in Nud1D to 0.91 in MorrL, and highest for Ontario, ranging from 0.97 in Nud1D to 0.98 to MorrL. The LST RMSD is generally lowest for Ontario, ranging from 1.62°C in MorrL to 1.71°C in Nud1Ddep, and highest for Erie, ranging from 1.45°C in Nud1D to 2.35°C in Nud1Ddep. Spatially varying bathymetry reduces the RMSD for Superior's LST by about 10% but increases it for Erie by roughly 60% (Figs. 12a,e), as evidence of the difficulty of tuning a simple 1D lake model to perform well for both deep and shallow lakes.

NU-WRF coupled to the 1D lake model generates excessive ice cover compared to the Great Lakes Environmental Research Laboratory–Great Lakes Ice Cover Database (Fig. 13). This 5-month mean bias in lake-average ice cover is modest for Erie, ranging from −1.7% in Nud1D to +7.4% in Nud1Ddep, and pronounced for Superior, ranging from +27.5% in MorrL to +39.9% in Nud1D. The model-versus-observed temporal correlation in daily ice cover is lowest for Superior, ranging from 0.63 in Nud1D to 0.80 in MorrL, and highest for Erie, ranging from 0.91 in Nud1Ddep to 0.97 in Nud1D (Fig. 13). The ice cover RMSD is relatively modest for Erie, ranging

Brought to you by MIT LIBRARIES | Unauthenticated | Downloaded 09/22/21 12:14 PM UTC

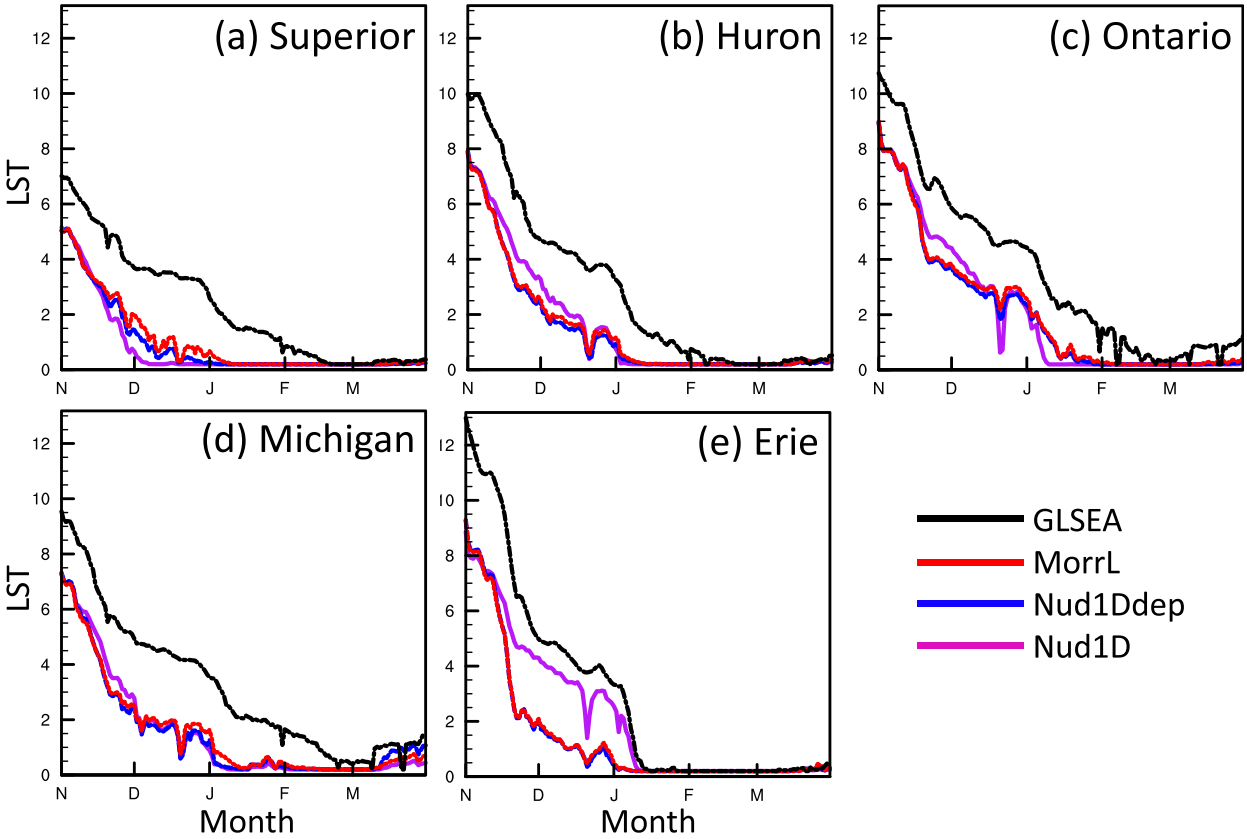

FIG. 12. Time series of daily lake surface temperature (°C) for Lakes (a) Superior, (b) Huron, (c) Ontario, (d) Michigan, and (e) Erie during November 2014–March 2015 from the Great Lakes Surface Environmental Analysis (GLSEA, black), MorrL (red), Nud1Ddep (blue), and Nud1D (purple).

from 11.1% in Nud1D to 20.3% in Nud1Ddep, and vast for Superior, ranging from 35.6% in MorrL to 50.8% in Nud1D. MorrL displays the lowest biases and RMSD and highest temporal correlations in ice cover, with the Morrison combination supporting higher, more realistic air and water temperatures. Lake Erie rapidly transitioned from a nearly ice-free state to almost full ice cover during January 2015, which was captured by the model in terms of rate, magnitude, and approximate timing (Fig. 13e). Lake Ontario underwent pronounced daily ice cover fluctuations, with an average observed day-to-day variation of 3.2%, while the model produces an overly smoothed time series with insufficient daily variations of 1.1% in Nud1D and 2.0% in MorrL (Fig. 13c); the model's excessively extensive and thick ice cover is inadequately sensitive to air temperature and wind speed variations. In NU-WRF, Superior ices up about 1–2 months too early and unrealistically remains mostly ice covered for much of the cold season (Fig. 13a). The results reinforce the limitations of using 1D lake models to simulate deep lakes' conditions.

e. Model assessment of overlake conditions

The time series of five overlake variables, namely, 2-m air temperature, surface incident downward solar radiation, 10-m wind speed, sensible heat flux, and latent heat flux, is contrasted between eight simulations (NoNud_Vary, Nud_Vary, NoNud, Nud, Nud1D, Nud1Ddep, MorrNoL, and MorrL) and Great Lakes Evaporation Network measurements for November 2014–March 2015 (Figs. 14 and 15). The analysis focuses on Stannard Rock (45.83°N, 85.15°W), Spectacle Reef (45.77°N, 84.15°W), Granite Island (46.72°N, 87.40°W), Long Point (42.57°N, 80.05°W), and White Shoal (45.83°N, 85.15°W), with results for Stannard Rock graphically presented (Fig. 14) for focused discussion. Model performance is best for MorrNoL and worst for Nud1D when considering all five overlake variables, five Great Lakes Evaporation Network sites, five months, and eight simulations.

An overlake atmospheric cold bias is simulated at all sites when averaged across the 5-month period, but most notably in January–March (Figs. 14a,d,g,j,m). Nudging and seasonally varying LSTs reduce this bias, yet lake model activation greatly amplifies it. While coupling NU-WRF to the 1D lake model permits inclusion of key lake–atmosphere interactions, it results in worse air temperature simulations than using Global Data Assimilation System skin temperatures as lake surface boundary conditions. Averaged among the Great Lakes Evaporation Network sites, the Morrison combination reduces

Brought to you by MIT LIBRARIES | Unauthenticated | Downloaded 09/22/21 12:14 PM UTC

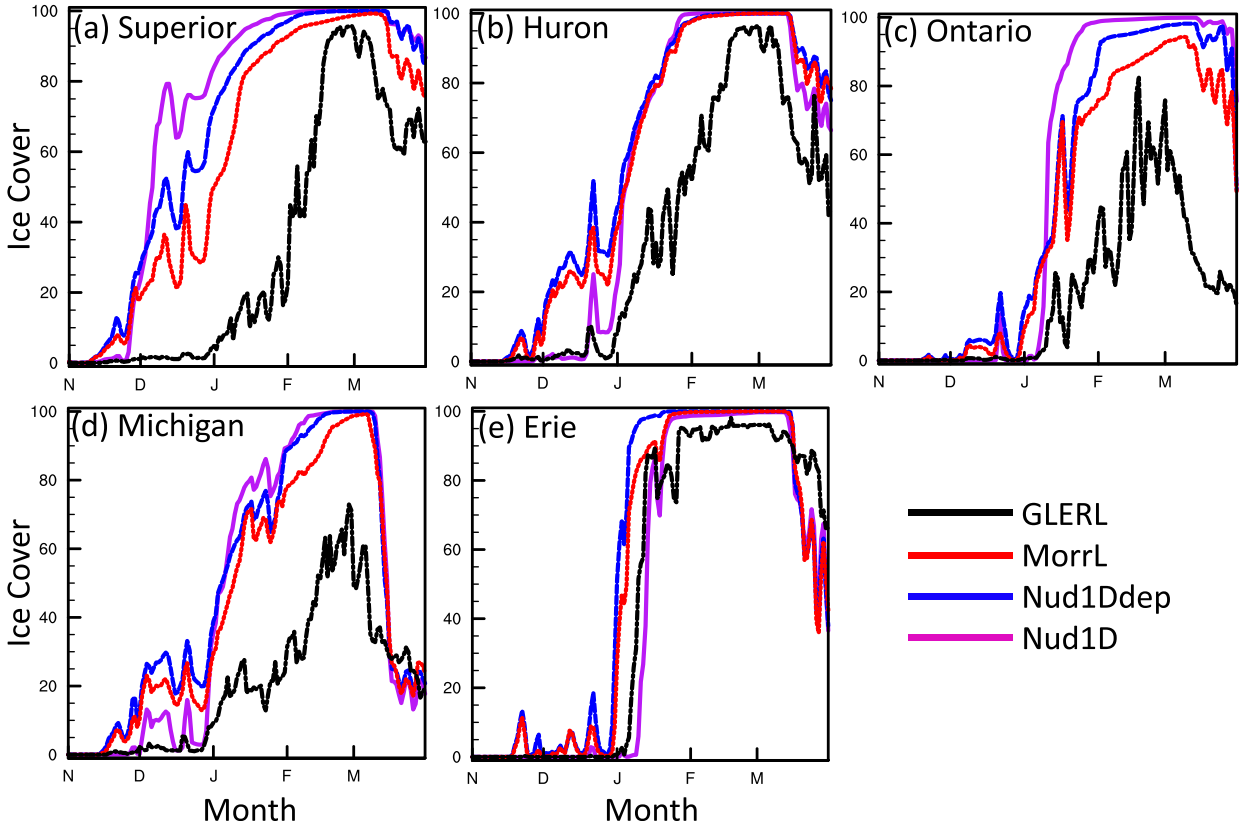

FIG. 13. Time series of daily percent ice cover for Lakes (a) Superior, (b) Huron, (c) Ontario, (d) Michigan, and (e) Erie during November 2014–March 2015 from the GLERL Great Lakes Ice Cover Database (black), MorrL (red), Nud1Ddep (blue), and Nud1D (purple).

the atmospheric cold bias by roughly 1/4th when the lake model is active. Regarding Stannard Rock's overlake air temperature simulation, the bias ranges from −7.0°C in Nud1D to −1.7°C in MorrNoL, temporal correlation ranges from 0.87 in MorrL to 0.97 in NudVary, and RMSD ranges from 2.4°C in MorrNoL to 8.4°C in Nud1D, indicating better performance without the lake model (Figs. 14a,d,g,j,m). The MorrL-simulated overlake conditions are more consistent with the Great Lakes Evaporation Network observations, in terms of bias, temporal correlation, and RMSD at Long Point (bias = −3.6°C) on Lake Erie and White Shoal (−3.5°C) on Lake Michigan and least consistent at Stannard Rock (−4.4°C) on Lake Superior.

Likely related to insufficient lake-effect-induced atmospheric moisture and cloud cover, NU-WRF produces excessive overlake shortwave radiation (Figs. 14b,e,h,k,n). At Stannard Rock, the bias ranges from $-0.3\,\mathrm{W\,m^{-2}}$ in NoNud to $+37.2\,\mathrm{W\,m^{-2}}$ in Nud1D, temporal correlation ranges from 0.46 in NoNud to 0.76 in MorrNoL, and RMSD ranges from $31.3\,\mathrm{W\,m^{-2}}$ in Nud to $46.3\,\mathrm{W\,m^{-2}}$ in Nud1D. The Morrison combination reduces the excessive overlake shortwave bias by 40% when the lake model is active. The simulated overlake wind speeds are too weak compared to the Great Lakes Evaporation Network observations. Stannard Rock's bias in 10-m wind speed ranges from $-3.6\,\mathrm{m\,s^{-1}}$ in Nud1D to $-1.5\,\mathrm{m\,s^{-1}}$ in Nud and temporal correlation ranges from 0.76 in NoNudVary to 0.82 in NudVary.

The Great Lakes Evaporation Network dataset provides valuable insights into overlake turbulent fluxes, applied here to evaluate NU-WRF's credibility. NU-WRF produces insufficient turbulent fluxes over Lakes Superior (Granite Island and Stannard Rock) and Huron (Spectacle Reef), coinciding with the greatest underestimation of near-surface wind speeds, and excessive turbulent fluxes over shallow Lake Erie (Long Point) (Figs. 14 and 15). Compared to observed sensible heat fluxes at Stannard Rock, the model bias varies from $-70.9\,\mathrm{W\,m^{-2}}$ in Nud1D to $-15.4\,\mathrm{W\,m^{-2}}$ in NoNudVary, temporal correlation varies from 0.19 in Nud1Ddep to 0.75 in MorrNoL, and RMSD varies from $49.9\,\mathrm{W\,m^{-2}}$ in MorrNoL to $109.4\,\mathrm{W\,m^{-2}}$ in Nud1Ddep (Figs. 15a,c,e,g,i). Temporally varying LSTs reduce the sensible heat flux bias from Nud and NoNud. Lake model coupling leads to sensible heat fluxes that are insufficient over Superior and excessive over Erie. Compared to observed latent heat fluxes at Stannard Rock, the bias ranges from $-90.5\,\mathrm{W\,m^{-2}}$ in Nud1D to $+12.3\,\mathrm{W\,m^{-2}}$ in NoNud, temporal correlation ranges from 0.21 in Nud1Ddep to 0.68 in Nud, and RMSD ranges from $84.8\,\mathrm{W\,m^{-2}}$ in Nud to $119.0\,\mathrm{W\,m^{-2}}$ in Nud1D (Figs. 15b,d,f,h,j). Simulated LH fluxes (Fig. 15) are insufficient over Superior and Huron given excessive ice cover (Fig. 13).

Brought to you by MIT LIBRARIES | Unauthenticated | Downloaded 09/22/21 12:14 PM UTC

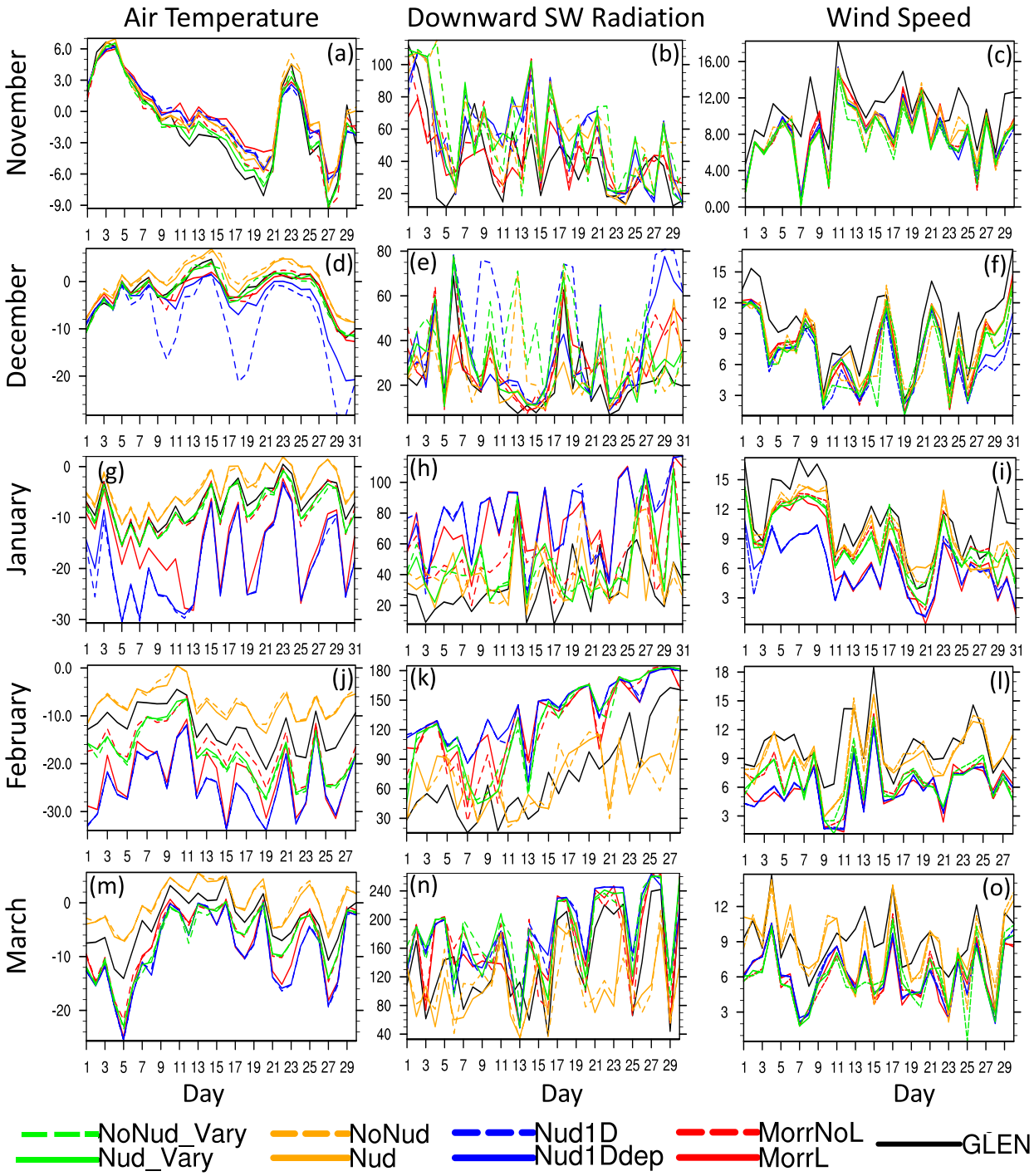

FIG. 14. Time series of daily (left) 2-m air temperature (°C), (center) downward surface shortwave radiation (W m^{-2}), and (right) 10-m wind speed for (a)–(c) November 2014, (d)–(f) December 2014, (g)–(i) January 2015, (j)–(l) February 2015, and (m)–(o) March 2015 at Stannard Rock based on Great Lakes Evaporation Network (GLEN) observations and eight NU-WRF model simulations.

4. Discussion and conclusions

The 3-km NU-WRF ensemble for the Great Lakes Basin for November 2014–March 2015 yields the following conclusions regarding model performance and impacts of parameterization selection, while noting the limitation of the study by focusing on a single cold season.

- Consistent with studies by Bonan (1995), Lofgren (1997), and Notaro et al. (2013a), the Great Lakes impose a

Brought to you by MIT LIBRARIES | Unauthenticated | Downloaded 09/22/21 12:14 PM UTC

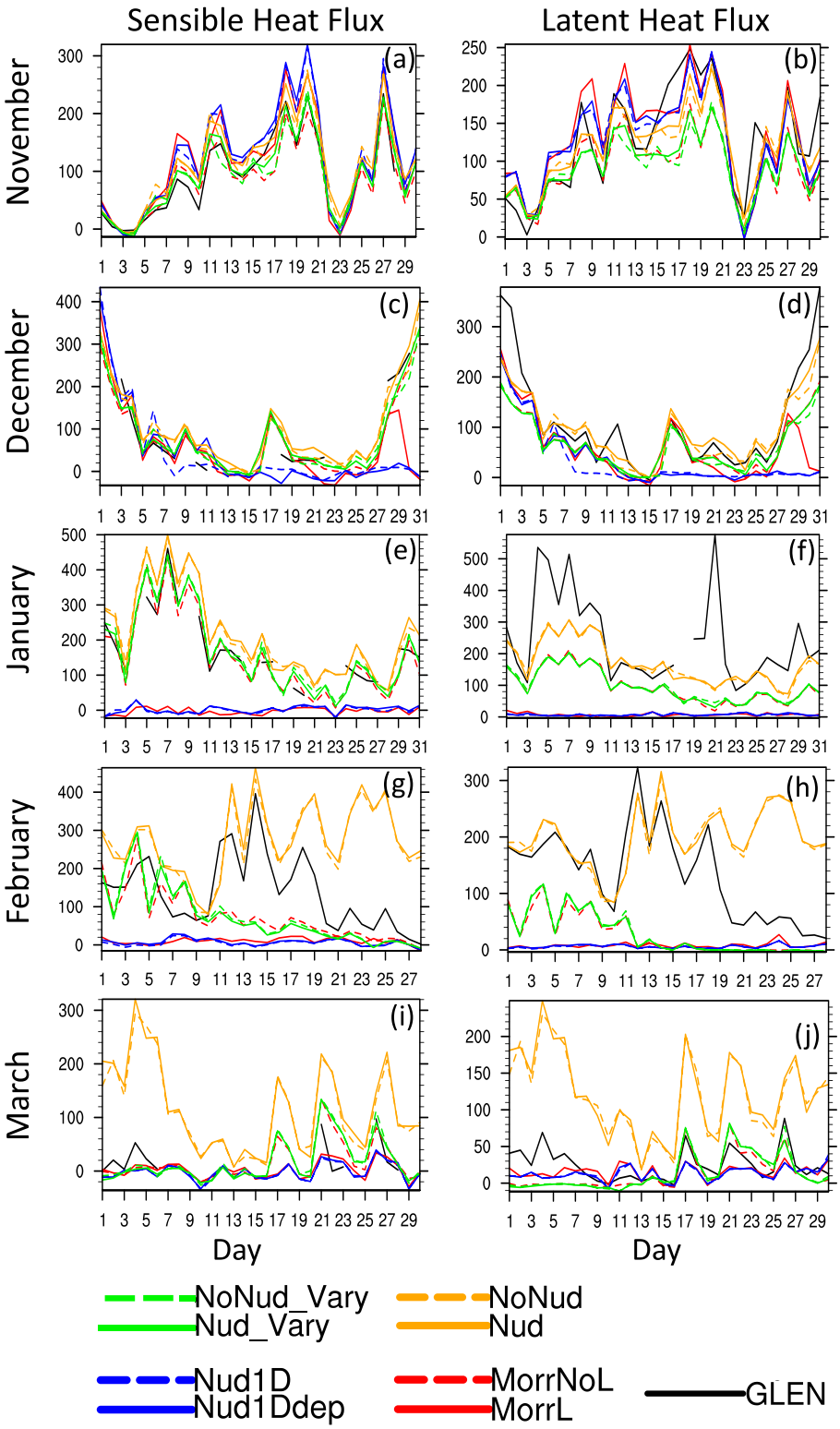

FIG. 15. Time series of daily (left) sensible heat flux (W m^{-2}) and (right) latent heat flux (W m^{-2}) for (a),(b) November 2014, (c),(d) December 2014, (e),(f) January 2015, (g),(h) February 2015, and (i),(j) March 2015 at Stannard Rock based on Great Lakes Evaporation Network (GLEN) observations and eight NU-WRF model simulations.

Brought to you by MIT LIBRARIES | Unauthenticated | Downloaded 09/22/21 12:14 PM UTC

pronounced influence on cold season climate across the surrounding states. Accurate lake representation is critical to correctly simulate the Midwest and Northeast United States' climatology.

- NU-WRF has an intrinsic atmospheric cold bias across the Great Lakes Basin during the cold season, as also noted in WRF by Mallard et al. (2014) and D'Orgeville et al. (2014). As noted here and by Mallard et al. (2014), coupling WRF to a 1D lake model amplifies the cold atmospheric bias due to LST and ice cover biases. The Morrison combination helps alleviate the atmospheric cold bias (likely by enhancing cloud cover and downward longwave radiation), consistent with Mooney et al. (2013) and D'Orgeville et al. (2014) who conclude that the RRTM longwave radiation scheme, MYNN boundary layer scheme, and Morrison's microphysics scheme improve winter air temperature simulations.
- NU-WRF generates excessive cold season precipitation, with too few dry days and too many heavy precipitation days. Mallard et al. (2014) likewise identified a WRF wet bias in this region, extending across the entire annual cycle. Furthermore, the region's cold season wet bias emerged in WRF experiments by D'Orgeville et al. (2014) and Sharma et al. (2019); the latter study determined that WRF failed to produce enough cold-season dry days, as also seen here. The simulated wintertime excessive precipitation bias in the Great Lakes region is not restricted to WRF, as Basile et al. (2017) identified the same persistent bias in all 12 examined Coupled Model Intercomparison Project Phase Five models and all 10 examined North American Regional Climate Change Assessment Program regional climate models. The cause of this regional bias across models remains uncertain, although Basile et al. (2017) hypothesized that observed wintertime precipitation measurements in this region might suffer significantly from gauge error associated with solid phase precipitation and wind-induced undercatch (Legates and Willmott 1990) due to very high snow-to-liquid precipitation ratios (light-weighted snow particles that more easily blow around gauges) especially in common lake-effect locations (Baxter et al. 2005). In fact, based on data presented by Adam and Lettenmaier (2003), the mean precipitation catch ratio for the Great Lakes region for November–March is only 76%, such that correcting the NLDAS-2 precipitation with this catch ratio would greatly amplify the actual observed precipitation rates and eliminate the apparent NU-WRF-simulated wet bias. NU-WRF-simulated surface insolation is excessive in the region, and despite the positive precipitation bias, low-level specific humidity is insufficient; the Morrison combination helps reduce the solar radiation biases. This finding is consistent with WRF studies by Martínez-Castro et al. (2019), which found that the Morrison scheme better resolved convective cloud features, and Orr et al. (2017), which found that the Morrison scheme improved cloud cover and reduced excessive surface incident shortwave radiation. Here, the Morrison combination improves most performance statistics related to wind and air temperature yet degrades the simulated precipitation.
- NU-WRF's cold season precipitation across the Great Lakes Basin is sensitive to seasonally varying LSTs and nudging and mostly insensitive to microphysics scheme and 1D lake model coupling. Likewise, Nicholls et al. (2017) and Lim et al. (2020) found that the choice of cloud microphysics scheme did not substantially impact precipitation distribution and intensity for United States nor'easters or Korean snowstorms, respectively. While Conrick et al. (2015) found a large sensitivity of WRF-simulated precipitation to boundary layer scheme during a single lake-effect snowstorm, this sensitivity is minimal when averaged in space and time across the Great Lakes Basin for the current paper's month-long simulations (e.g., comparing Nud1Ddep with the Yonsei University boundary layer scheme, PBLMYJ with the Mellow–Yamada–Janjić boundary layer scheme, and SFC_MYNN with the Mellor–Yamada–Nakanishi–Niino boundary layer scheme).
- The present study demonstrates the benefits of spectral nudging, which increases the model-versus-observed temporal correlations for all analyzed fields, particularly precipitation and physical snow depth. Prior WRF studies have produced a spectrum of detrimental to beneficial impacts from spectral nudging, including degraded United States precipitation simulations by Bowden et al. (2012, 2013), Otte et al. (2012), and Spero et al. (2014); relative insensitivity of simulated United States' precipitation amounts to spectral nudging strength by Bullock et al. (2014); and reduced East Asian temperature and precipitation biases by Ma et al. (2016) and Tang et al. (2017). Here, nudging improves the spatial patterns of snowfall and snow depth, including reducing Ontario's negative bias in liquid-equivalent snow depth.
- Alexandru et al. (2009) and Glisan et al. (2013) expressed concern that strong nudging can reduce or filter out extreme meteorological events by pushing a regional climate model toward a smoother large-scale atmospheric state. Here, spectral nudging reduces the cold-season frequency of heavy precipitation days, although this modification of the probability density function of daily precipitation increases the consistency with observations.
- Model-versus-observed temporal correlations during the cold season are typically highest for pressure, wind, specific humidity, and air temperature, likely due to these variables' inclusion in the lateral boundary conditions and spectral nudging, and lowest for surface incident shortwave radiation and overland turbulent fluxes. These findings are consistent with WRF studies by Mooney et al. (2013) and Boulard et al. (2016), which identified higher temporal correlations with observations for air temperature, precipitation, and wind speed and lower correlations for humidity and shortwave radiation.
- Fall turnover initiates too early in the model, leading to a wintertime cold LST bias, as also noted by Mallard et al. (2014) using WRF coupled to a 1D lake model. The model-versus-observed temporal correlation in LST is highest for Ontario and lowest for Superior and in percent ice cover is highest for Erie and lowest for Superior. Lake Superior's ice season initiates 1–2 months too early in NU-WRF coupled to the 1D lake model. Prior studies have concluded that 1D lake models perform best for shallow lakes (Martynov et al. 2010;

Brought to you by MIT LIBRARIES | Unauthenticated | Downloaded 09/22/21 12:14 PM UTC

Samuelsson et al. 2010; Bennington et al. 2014; Mallard et al. 2014), with inferior results for deep Superior. Mallard et al. (2014) determined that the LST and ice cover performance of WRF coupled to the Freshwater Lake Model was best for Erie and worst for Superior, with excessive Superior ice cover. Here, the inferior performance of the 1D lake model in NU-WRF over deep Lake Superior generally leads to the greatest biases in LST, ice cover, overlake air temperature, and lake evaporation among the Great Lakes.

- The Morrison combination improves ice cover biases, RMSD, and temporal correlations by dampening the atmospheric model's regional cold bias and supporting more realistic cold season LSTs.
- NU-WRF coupled to the 1D lake model underpredicts cold season evaporation over Lakes Superior and Huron, related to excessive ice cover, cooler-than-observed water temperatures, and insufficient wind speeds.
- Based on comparison of NU-WRF simulations coupled to the 1D lake model with either fixed 50-m uniform lake depths (Nud1D) or spatially variable lake depths (Nud1Ddep), use of a constant 50-m lake depth for all lake grid cells, as commonly done in earlier generations of lake models, leads to substantial impacts over, and in close proximity to, the lakes, but not much impact when averaged across the inner domain. Uniform lake depth results in 1–2.5°C higher LSTs on shallow Lake Erie (actual mean depth = 19 m) in mid–November to early January and over 0.5°C lower LSTs on deep Lake Superior (actual mean depth = 147 m) in late November to mid–December. Furthermore, uniform lake depth leads to 20%–90% less ice cover on Lake Erie during early to mid-January, with a delayed onset of the ice season, and 10%–30% greater ice cover on Lake Superior. In response to these LST and ice cover responses to uniform 50-m lake depths, overlake turbulent fluxes are greatly enhanced over Lake Erie, with November–March mean sensible and latent heat fluxes at Long Point (on Lake Erie) increased by 20.6 and 14.6 $W\,m^{-2}$, respectively, but only modestly impacted over Lake Superior. The enhanced turbulent fluxes over Lake Erie support 30%–60% greater precipitation over and downwind of the lake during January 2015. These findings regarding the impacts of uniform versus spatially varying lake bathymetry on LST and ice cover are highly consistent with the results of Qiu et al. (2020).

While NU-WRF's coupling to a 1D lake model is a critical achievement for representing lake–atmosphere interactions and their role in climate change, the 1D lake model degrades many aspects of the simulated regional climate. However, the authors do not recommend that climate modelers proceed without inclusion of a representation of lake physics in their models. Rather, further efforts are needed to incorporate 3D lake models into high-resolution regional climate models to improve spatiotemporal patterns of LST, ice cover, and lake–atmosphere interactions. As a result of this modeling need, the authors developed an advanced modeling tool for large lake basins, consisting of NU-WRF, with nested domains down to 3 km, interactively coupled to the Finite Volume Community Ocean Model [this ocean model, run offline by Fujisaki-Manome et al. (2017), successfully simulates overlake turbulent fluxes] to represent 3D lake hydrodynamics.

Acknowledgments. The study was funded by NASA's Modeling, Analysis, and Prediction Program (Grant 80NSSC17K0291 and Grant 80NSSC17K0287) and a sub-contract from NOAA's Great Lakes Integrated Sciences and Assessments Program. Computational resources were provided through NASA's Center for Climate Simulation. The authors gratefully acknowledge partial support from the Illinois State Water Survey at the University of Illinois at Urbana–Champaign. Opinions expressed are those of the authors and not necessarily those of their institutions.

REFERENCES

Adam, J. C., and D. P. Lettenmaier, 2003: Adjustment of global gridded precipitation for systematic bias. *J. Geophys. Res.*, **108**, 4257, https://doi.org/10.1029/2002JD002499.

Alexandru, A., R. de Elia, R. Laprise, L. Separovic, and S. Biner, 2009: Sensitivity study of regional climate model simulations to large-scale nudging parameters. *Mon. Wea. Rev.*, **137**, 1666–1686, https://doi.org/10.1175/2008MWR2620.1.

Assel, R. A., 2005: Classification of annual Great Lakes ice cycles: Winters of 1973-2002. *J. Climate*, **18**, 4895–4905, https://doi.org/10.1175/JCLI3571.1.

——, D. C. Norton, and K. C. Cronk, 2002: A Great Lakes ice cover digital data set for winters 1973-2000. NOAA Tech. Memo. GLERL-121, 46 pp., https://www.glerl.noaa.gov/pubs/tech_reports/glerl-121/tm-121.pdf.

——, J. Wang, A. Clites, and X. Bai, 2013: Analysis of Great Lakes ice cover climatology: Winters 2006-2011. NOAA Tech. Memo. GLERL-157, 26 pp., https://www.glerl.noaa.gov/pubs/tech_reports/glerl-157/tm-157.pdf.

Austin, J., and S. Colman, 2007: Lake Superior summer water temperatures are increasing more rapidly than regional air temperatures: A positive ice–albedo feedback. *Geophys. Res. Lett.*, **34**, L06604, https://doi.org/10.1029/2006GL029021.

Azar, A. E., H. Ghedira, P. Romanov, S. Mahani, M. Tedesco, and R. Khanbilvardi, 2008: Application of satellite microwave images in estimating snow water equivalent. *J. Amer. Water Resour. Assoc.*, **44**, 1347–1362, https://doi.org/10.1111/j.1752-1688.2008.00227.x.

Bard, L., and D. A. R. Kristovich, 2012: Trend reversal in Lake Michigan contribution to snowfall. *J. Appl. Meteor. Climatol.*, **51**, 2038–2046, https://doi.org/10.1175/JAMC-D-12-064.1.

Barker, H., J. N. S. Cole, J.-J. Morcrette, R. Pincus, and P. Raisanen, 2007: Monte Carlo Independent Column Approximation (McICA): Up and running in North America and Europe. *17th Atmospheric Radiation Measurement (ARM) Science Team Meeting*, Monterey, CA, U.S. DOE, https://clouds.eos.ubc.ca/~phil/docs/0327_barker.pdf.

Barrett, A. P., 2003: National Operational Hydrologic Remote Sensing Center Snow Data Assimilation System (SNODAS) products at NSIDC. NSDIC Special Rep. 11, 19 pp., https://nsidc.org/sites/nsidc.org/files/files/nsidc_special_report_11.pdf.

Basile, S. J., S. A. Rauscher, and A. L. Steiner, 2017: Projected precipitation changes within the Great Lakes and western Lake Erie Basin: A multi-model analysis of intensity and seasonality. *Int. J. Climatol.*, **37**, 4864–4879, https://doi.org/10.1002/joc.5128.

Bates, G. T., F. Giorgi, and S. W. Hostetler, 1993: Toward the simulation of the effects of the Great Lakes on regional climate. *Mon. Wea. Rev.*, **121**, 1373–1387, https://doi.org/10.1175/1520-0493(1993)121<1373:TTSOTE>2.0.CO;2.

Brought to you by MIT LIBRARIES | Unauthenticated | Downloaded 09/22/21 12:14 PM UTC

Baxter, M. A., C. E. Graves, and J. T. Moore, 2005: A climatology of snow-to-liquid ratio for the contiguous United States. *Wea. Forecasting*, **20**, 729–744, https://doi.org/10.1175/WAF856.1.

Behnke, R., S. Vavrus, A. Allstadt, T. Albright, W. E. Thogmartin, and V. C. Radeloff, 2016: Evaluation of downscaled, gridded climate data for the conterminous United States. *Ecol. Appl.*, **26**, 1338–1351, https://doi.org/10.1002/15-1061.

Beletsky, D., N. Hawley, Y. R. Rao, H. A. Vanderploeg, R. Beletsky, D. J. Schwab, and S. A. Ruberg, 2012: Summer thermal structure and anticyclonic circulation of Lake Erie. *Geophys. Res. Lett.*, **39**, L06605, https://doi.org/10.1029/2012GL051002.

Bennington, V., G. A. McKinley, N. Kimura, and C. H. Wu, 2010: General circulation of Lake Superior: Mean, variability, and trends from 1979 to 2006. *J. Geophys. Res.*, **115**, C12015, https://doi.org/10.1029/2010JC006261.

——, M. Notaro, and K. D. Holman, 2014: Improving climate sensitivity of deep lakes within a regional climate model and its impact on simulated climate. *J. Climate*, **27**, 2886–2911, https://doi.org/10.1175/JCLI-D-13-00110.1.

Blanken, P. D., C. Spence, N. Hedstrom, and J. D. Lenters, 2011: Evaporation from Lake Superior: 1. Physical controls and processes. *J. Great Lakes Res.*, **37**, 707–716, https://doi.org/10.1016/j.jglr.2011.08.009.

Bonan, G. B., 1995: Sensitivity of a GCM simulation to inclusion of inland water surfaces. *J. Climate*, **8**, 2691–2704, https://doi.org/10.1175/1520-0442(1995)008<2691:SOAGST>2.0.CO;2.

Botts, L., and B. Krushelnicki, 1988: *The Great Lakes: An Environmental Atlas and Resource Book*. U.S. Environmental Protection Agency, 46 pp.

Boulard, D., and Coauthors, 2016: Capability of a regional climate model to simulate climate variables requested for water balance computation: A case study over northeastern France. *Climate Dyn.*, **46**, 2689–2716, https://doi.org/10.1007/s00382-015-2724-9.

Bowden, J. H., T. L. Otte, C. G. Nolte, and M. J. Otte, 2012: Examining interior grid nudging techniques using two-way nesting in the WRF model for regional climate modeling. *J. Climate*, **25**, 2805–2823, https://doi.org/10.1175/JCLI-D-11-00167.1.

——, C. G. Nolte, and T. L. Otte, 2013: Simulating the impact of the large-scale circulation on the 2-m temperature and precipitation climatology. *Climate Dyn.*, **40**, 1903–1920, https://doi.org/10.1007/s00382-012-1440-y.

Briley, L. J., W. S. Ashley, R. B. Rood, and A. Krmenec, 2017: The role of meteorological processes in the description of uncertainty for climate change decision-making. *Theor. Appl. Climatol.*, **127**, 643–654, https://doi.org/10.1007/s00704-015-1652-2.

Brown, L. C., and C. R. Duguay, 2010: The response and role of ice cover in lake climate interactions. *Prog. Phys. Geogr.*, **34**, 671–704, https://doi.org/10.1177/0309133310375653.

Bullock, O. R., Jr., K. Alapaty, J. A. Herwehe, M. S. Mallard, T. L. Otte, R. C. Gilliam, and C. G. Nolte, 2014: An observation-based investigation of nudging in WRF for downscaling surface climate information to 12-km grid spacing. *J. Appl. Meteor. Climatol.*, **53**, 20–33, https://doi.org/10.1175/JAMC-D-13-030.1.

Burnett, A., M. Kirby, H. Mullins, and W. Patterson, 2003: Increasing Great Lake effect snowfall during the twentieth century: A regional response to global warming? *J. Climate*, **16**, 3535–3542, https://doi.org/10.1175/1520-0442(2003)016<3535:IGLSDT>2.0.CO;2.

Carroll, T., D. Cline, G. Fall, A. Nilsson, L. Li, and A. Rost, 2001: NOHRSC operations and the simulation of snow cover properties for the conterminous U.S. *Proc. 69th Annual Meeting of the Western Snow Conf.*, Sun Valley, ID, Western Snow Conference, 14 pp.

Changnon, S. A., Jr., and D. M. A. Jones, 1972: Review of the influences of the Great Lakes on weather. *Water Resour. Res.*, **8**, 360–371, https://doi.org/10.1029/WR008i002p00360.

Charusombat, U., and Coauthors, 2018: Evaluating and improving modeled turbulent heat fluxes across the North American Great Lakes. *Hydrol. Earth Syst. Sci.*, **22**, 5559–5578, https://doi.org/10.5194/hess-22-5559-2018.

Chen, C., H. Liu, and R. C. Beardsley, 2003: An unstructured, finite-volume, three-dimensional, primitive equation ocean model: Application to coastal ocean and estuaries. *J. Atmos. Oceanic Technol.*, **20**, 159–186, https://doi.org/10.1175/1520-0426(2003)020<0159:AUGFVT>2.0.CO;2.

Chen, F., and Y. Zhang, 2009: On the coupling strength between the land surface and the atmosphere: From viewpoint of surface exchange coefficients. *Geophys. Res. Lett.*, **36**, L10404, https://doi.org/10.1029/2009GL037980.

Chen, M. Y., W. Shi, P. P. Xie, V. B. S. Silva, V. E. Kousky, R. W. Higgins, and J. E. Janowiak, 2008: Assessing objective techniques for gauge-based analyses of global daily precipitation. *J. Geophys. Res.*, **113**, D04110, https://doi.org/10.1029/2007JD009132.

Chin, M., R. B. Rood, S.-J. Lin, J.-F. Miller, and A. Thompson, 2000: Atmospheric sulfur cycle simulated in the global model GOCART: Model description and global properties. *J. Geophys. Res.*, **105**, 24 671–24 687, https://doi.org/10.1029/2000JD900384.

Chou, M.-D., and M. J. Suarez, 1999: A solar radiation parameterization for atmospheric studies. Tech. Memo. NASA/TM-1999-104606, Vol. 15, 38 pp., http://gmao.gsfc.nasa.gov/pubs/docs/Chou136.pdf.

——, ——, X.-Z. Liang, and M. M.-H. Yan, 2001: A thermal infrared radiation parameterization for atmospheric studies. NASA/TM-2001-104606, Vol. 19, 54 pp., https://ntrs.nasa.gov/archive/nasa/casi.ntrs.nasa.gov/20010072848.pdf.

Chuang, H. Y., and P. J. Sousounis, 2003: The impact of the prevailing synoptic situation on the lake-aggregate effect. *Mon. Wea. Rev.*, **131**, 990–1010, https://doi.org/10.1175/1520-0493(2003)131<0990:TIOTPS>2.0.CO;2.

Clark, C. A., and Coauthors, 2020: Classification of Lake Michigan snow days for estimation of the lake-effect contribution to the downward trend in November snowfall. *Int. J. Climatol.*, **40**, 5656–5670, https://doi.org/10.1002/joc.6542.

Clow, D. W., L. Nanus, K. L. Verdin, and J. Schmidt, 2012: Evaluation of SNODAS snow depth and snow water equivalent estimates for the Colorado Rocky Mountains, USA. *Hydrol. Processes*, **26**, 2583–2591, https://doi.org/10.1002/hyp.9385.

Collins, W. D., and Coauthors, 2004: Description of the NCAR Community Atmosphere Model (CAM 3.0). NCAR Tech. Note NCAR/TN-464+STR, 214 pp., https://doi.org/10.5065/D63N21CH.

Colucci, S. J., 1976: Winter cyclone frequencies over the eastern United States and adjacent western Atlantic, 1964–1973. *Bull. Amer. Meteor. Soc.*, **57**, 548–553, https://doi.org/10.1175/1520-0477(1976)057<0548:WCFOTE>2.0.CO;2.

Conrick, R., H. D. Reeves, and S. Zhong, 2015: The dependence of QPF on the choice of boundary- and surface-layer parameterization for a lake-effect snowstorm. *J. Appl. Meteor. Climatol.*, **54**, 1177–1190, https://doi.org/10.1175/JAMC-D-14-0291.1.

Brought to you by MIT LIBRARIES | Unauthenticated | Downloaded 09/22/21 12:14 PM UTC

Crossman, E. J., and B. C. Cudmore, 1998: Biodiversity of the fishes of the Laurentian Great Lakes: A Great Lakes Fishery Commission project. *Ital. J. Zool.*, **65**, 357–361, https://doi.org/10.1080/11250009809386846.

Dai, A., K. E. Trenberth, and T. R. Karl, 1999: Effect of clouds, soil moisture, precipitation, and water vapor on diurnal temperature range. *J. Climate*, **12**, 2451–2473, https://doi.org/10.1175/1520-0442(1999)012<2451:EOCSMP>2.0.CO;2.

D'Orgeville, M., W. R. Peltier, A. R. Erler, and J. Gula, 2014: Climate change impacts on Great Lakes Basin precipitation extremes. *J. Geophys. Res. Atmos.*, **119**, 10 799–10 812, https://doi.org/10.1002/2014JD021855.

Easterling, D. R., G. A. Meehl, C. Parmesan, S. A. Changnon, T. R. Karl, and L. O. Mearns, 2000: Climate extremes: Observations, modeling, and impacts. *Science*, **289**, 2068–2074, https://doi.org/10.1126/science.289.5487.2068.

Eichenlaub, V. L., 1979: *Weather and Climate of the Great Lakes Region*. University of Notre Dame Press, 335 pp.

Ellis, A. W., and J. J. Johnson, 2004: Hydroclimatic analysis of snowfall trends associated with the North American Great Lakes. *J. Hydrometeor.*, **5**, 471–486, https://doi.org/10.1175/1525-7541(2004)005<0471:HAOSTA>2.0.CO;2.

Ferraro, R., D. Waliser, and C. Peters-Lidard, 2017: NASA Downscaling Project Final Report. NASA/TP-2017-219579, 52 pp., https://trs.jpl.nasa.gov/handle/2014/45705.

Fujisaki, A., J. Wang, H. Hu, D. J. Schwab, N. Hawley, and Y. R. Rao, 2013: A modeling study of ice–water processes for Lake Erie applying coupled ice-circulation models. *J. Great Lakes Res.*, **38**, 585–599, https://doi.org/10.1016/j.jglr.2012.09.021.

Fujisaki-Manome, A., and Coauthors, 2017: Turbulent heat fluxes during an extreme lake-effect snow event. *J. Hydrometeor.*, **18**, 3145–3163, https://doi.org/10.1175/JHM-D-17-0062.1.

Glisan, J. M., W. J. Gutowski, J. J. Cassano, and M. E. Higgins, 2013: Effects of spectral nudging in WRF on Arctic temperature and precipitation simulations. *J. Climate*, **26**, 3985–3999, https://doi.org/10.1175/JCLI-D-12-00318.1.

Grell, G. A., S. E. Peckham, S. McKeen, R. Schmitz, G. Frost, W. C. Skamarock, and B. Eder, 2005: Fully coupled "online" chemistry within the WRF model. *Atmos. Environ.*, **39**, 6957–6975, https://doi.org/10.1016/j.atmosenv.2005.04.027.

Gronewold, A. D., V. Fortin, B. Lofgren, A. Clites, C. A. Stow, and F. Quinn, 2013: Coasts, water levels, and climate change: A Great Lakes perspective. *Climatic Change*, **120**, 697–711, https://doi.org/10.1007/s10584-013-0840-2.

Gu, H., J. Jin, Y. Wu, M. B. Ek, and Z. M. Subin, 2015: Calibration and validation of lake surface temperature simulations with the coupled WRF-lake model. *Climatic Change*, **129**, 471–483, https://doi.org/10.1007/s10584-013-0978-y.

Gula, J., and W. R. Peltier, 2012: Dynamical downscaling over the Great Lakes Basin of North America using the WRF regional climate model: The impact of the Great Lakes system on regional greenhouse warming. *J. Climate*, **25**, 7723–7742, https://doi.org/10.1175/JCLI-D-11-00388.1.

Hartnett, J. J., J. M. Collins, M. A. Baxter, and D. P. Chambers, 2014: Spatiotemporal snowfall trends in central New York. *J. Appl. Meteor. Climatol.*, **53**, 2685–2697, https://doi.org/10.1175/JAMC-D-14-0084.1.

Hay, L. E., G. H. Leavesley, M. P. Clark, S. L. Markstrom, R. J. Viger, and M. Umemoto, 2006: Step wise, multiple objective calibration of a hydrologic model for a snowmelt dominated basin. *J. Amer. Water Resour. Assoc.*, **42**, 877–890, https://doi.org/10.1111/j.1752-1688.2006.tb04501.x.

Higgins, R. W., J. E. Janowiak, and Y. Yao, 1996: A gridded hourly precipitation data base for the United States (1963–1993). NCEP/Climate Prediction Center Atlas 1, NOAA, 47 pp., http://www.cpc.ncep.noaa.gov/research_papers/ncep_cpc_atlas/1/cover.html.

Hong, S.-Y., S. Y. Noh, and J. Dudhia, 2006: A new vertical diffusion package with an explicit treatment of entrainment processes. *Mon. Wea. Rev.*, **134**, 2318–2341, https://doi.org/10.1175/MWR3199.1.

——, K.-S. S. Lim, Y.-H. Lee, J.-C. Ha, H.-W. Kim, S.-J. Ham, and J. Dudhia, 2010: Evaluation of the WRF double-moment 6-class microphysics scheme for precipitating convection. *Adv. Meteor.*, **2010**, 707253, https://doi.org/10.1155/2010/707253.

Iacono, M. J., J. S. Delamere, E. J. Mlawer, M. W. Shephard, S. A. Clough, and W. D. Collins, 2008: Radiative forcing by long-lived greenhouse gases: Calculations with the AER radiative transfer models. *J. Geophys. Res.*, **113**, D13103, https://doi.org/10.1029/2008JD009944.

Iguchi, T., and Coauthors, 2017: Sensitivity of CONUS summer rainfall to the selection of cumulus parameterization schemes in NU-WRF seasonal simulations. *J. Hydrometeor.*, **18**, 1689–1706, https://doi.org/10.1175/JHM-D-16-0120.1.

Insua-Costa, D., and G. Miguez-Macho, 2018: A new moisture tagging capability in the Weather Research and Forecasting model: Formulation, validation and application to the 2014 Great Lake-effect snowstorm. *Earth Syst. Dyn.*, **9**, 167–185, https://doi.org/10.5194/esd-9-167-2018.

Janjić, Z. I., 1990: The step-mountain coordinate: Physical package. *Mon. Wea. Rev.*, **118**, 1429–1443, https://doi.org/10.1175/1520-0493(1990)118<1429:TSMCPP>2.0.CO;2.

——, 1994: The step-mountain Eta coordinate model: Further developments of the convection, viscous layer, and turbulence closure schemes. *Mon. Wea. Rev.*, **122**, 927–945, https://doi.org/10.1175/1520-0493(1994)122<0927:TSMECM>2.0.CO;2.

——, 2001: Nonsingular implementation of the Mellor-Yamada level 2.5 scheme in the NCEP Meso model. NCEP Office Note 437, 61 pp.

Jiménez, P. A., J. Dudhia, J. F. González-Rouco, J. Navarro, J. P. Montávez, and E. García-Bustamante, 2012: A revised scheme for the WRF surface layer formulation. *Mon. Wea. Rev.*, **140**, 898–918, https://doi.org/10.1175/MWR-D-11-00056.1.

Kain, J. S., 2004: The Kain–Fritsch convective parameterization: An update. *J. Appl. Meteor.*, **43**, 170–181, https://doi.org/10.1175/1520-0450(2004)043<0170:TKCPAU>2.0.CO;2.

——, and J. M. Fritsch, 1990: A one-dimensional entraining/detraining plume model and its application in convective parameterization. *J. Atmos. Sci.*, **47**, 2784–2802, https://doi.org/10.1175/1520-0469(1990)047<2784:AODEPM>2.0.CO;2.

King, F., A. R. Erler, S. K. Frey, and C. G. Fletcher, 2020: Application of machine learning techniques for regional bias correction of snow water equivalent estimates in Ontario, Canada. *Hydrol. Earth Syst. Sci.*, **24**, 4887–4902, https://doi.org/10.5194/hess-24-4887-2020.

Kling, G. W., and Coauthors, 2003: *Confronting Climate Change in the Great Lakes Region: Impacts on Our Communities and Ecosystems*. Union of Concerned Scientists and Ecological Society of America, 92 pp.

Kourzeneva, E., 2010: External data for lake parameterization in numerical weather prediction and climate modeling. *Boreal Environ. Res.*, **15**, 165–177.

Kristovich, D. A. R., and R. A. Steve III, 1995: A satellite study of cloud-band frequencies over the Great Lakes. *J. Appl.*

Brought to you by MIT LIBRARIES | Unauthenticated | Downloaded 09/22/21 12:14 PM UTC

Meteor., **34**, 2083–2090, https://doi.org/10.1175/1520-0450(1995)034<2083:ASSOCB>2.0.CO;2.

——, and R. R. Braham Jr., 1998: Mean profiles of moisture fluxes in snow-filled boundary layers. *Bound.-Layer Meteor.*, **87**, 195–215, https://doi.org/10.1023/A:1000836401204.

——, and N. F. Laird, 1998: Observations of widespread lake-effect cloudiness: Influences of lake surface temperature and upwind conditions. *Wea. Forecasting*, **13**, 811–821, https://doi.org/10.1175/1520-0434(1998)013<0811:OOWLEC>2.0.CO;2.

Kumar, S. V., and Coauthors, 2006: Land information system: An interoperable framework for high resolution land surface modeling. *Environ. Modell. Software*, **21**, 1402–1415, https://doi.org/10.1016/j.envsoft.2005.07.004.

Kunkel, K. E., D. R. Easterling, K. Redmond, and K. Hubbard, 2003: Temporal variations of extreme precipitation events in the United States: 1895–2000. *Geophys. Res. Lett.*, **30**, 1900, https://doi.org/10.1029/2003GL018052.

——, L. Ensor, M. Palecki, D. Easterling, D. Robinson, K. G. Hubbard, and K. Redmond, 2009: A new look at lake-effect snowfall trends in the Laurentian Great Lakes using a temporally homogeneous data set. *J. Great Lakes Res.*, **35**, 23–29, https://doi.org/10.1016/j.jglr.2008.11.003.

——, D. R. Easterling, D. A. R. Kristovich, B. Gleason, L. Stoecker, and R. Smith, 2012: Meteorological causes of the secular variations in observed extreme precipitation events for the conterminous United States. *J. Hydrometeor.*, **13**, 1131–1141, https://doi.org/10.1175/JHM-D-11-0108.1.

——, and Coauthors, 2013: Regional climate trends and scenarios for the U.S. National Climate Assessment: Part 3—Climate of the Midwest U.S., NOAA Tech. Rep. NESDIS 142-3, 103 pp., http://www.nesdis.noaa.gov/technical_reports/NOAA_NESDIS_Tech_Report_142-3-Climate_of_the_Midwest_U.S.pdf.

Lee, H., D. E. Waliser, R. Ferraro, T. Iguchi, C. D. Peters-Lidard, B. Tian, P. C. Loikith, and D. B. Wright, 2017: Evaluating hourly rainfall characteristics over the U.S. Great Plains in dynamically downscaled climate model simulations using NASA-Unified WRF. *J. Geophys. Res. Atmos.*, **122**, 7371–7384, https://doi.org/10.1002/2017JD026564.

Legates, D. R., and C. J. Willmott, 1990: Mean seasonal and spatial variability in gauge-corrected, global precipitation. *Int. J. Climatol.*, **10**, 111–127, https://doi.org/10.1002/joc.3370100202.

Lenters, J. D., J. B. Anderton, P. D. Blanken, C. Spence, and A. E. Suyker, 2013: Assessing the impacts of climate variability and change on Great Lakes evaporation: Implications for water levels and the need for a coordinated observation network. GLISA 2011 Project Rep., 11 pp., http://glisa.umich.edu/media/files/projectreports/GLISA_ProjRep_Lake_Evaporation.pdf.

Li, X., W. Pichel, P. Clemente-Colon, V. Krasnopolosky, and J. Sapper, 2001: Validation of coastal sea and lake surface temperature measurements derived from NOAA/AVHRR data. *Int. J. Remote Sens,* **22**, 1285–1303, https://doi.org/10.1080/01431160151144350.

Lim, K.-S. S., E.-C. Chang, R. Sun, K. Kim, F. J. Tapiador, and G. Lee, 2020: Evaluation of simulated winter precipitation using WRF-ARW during the ICE-POP 2018 field campaign. *Wea. Forecasting*, **35**, 2199–2213, https://doi.org/10.1175/WAF-D-19-0236.1.

Lofgren, B. M., 1997: Simulated effects of idealized Laurentian Great Lakes on regional and large-scale climate. *J. Climate*, **10**, 2847–2858, https://doi.org/10.1175/1520-0442(1997)010<2847:SEOILG>2.0.CO;2.

——, 2014: Simulation of atmospheric and lake conditions in the Laurentian Great Lakes region using the Coupled Hydrosphere–Atmosphere Research Model (CHARM). NOAA Tech. Memo. GLERL-165, 23 pp., https://www.glerl.noaa.gov/pubs/tech_reports/glerl-165/tm-165.pdf.

Loikith, P., D. E. Waliser, J. Kim, and R. Ferraro, 2018: Evaluation of cool season precipitation event characteristics over the Northeast US in a suite of downscaled climate model hindcasts. *Climate Dyn.*, **50**, 3711–3727, https://doi.org/10.1007/s00382-017-3837-0.

Ma, Y., Y. Yang, X. Mai, C. Qui, X. Long, and C. Wang, 2016: Comparison of analysis and spectral nudging techniques for dynamical downscaling with the WRF model over China. *Adv. Meteor.*, **2016**, 4761513, https://doi.org/10.1155/2016/4761513.

Mallard, M. S., C. G. Nolte, O. R. Bullock, T. L. Spero, and J. Gula, 2014: Using a coupled lake model with WRF for dynamical downscaling. *J. Geophys. Res. Atmos.*, **119**, 7193–7208, https://doi.org/10.1002/2014JD021785.

——, ——, T. L. Spero, O. R. Bullock, K. Alapaty, J. A. Herwehe, J. Gula, and J. H. Bowden, 2015: Technical challenges and solutions in representing lakes when using WRF in downscaling applications. *Geosci. Model Dev.*, **8**, 1085–1096, https://doi.org/10.5194/gmd-8-1085-2015.

Manabe, S., and R. T. Wetherald, 1967: Thermal equilibrium of the atmosphere with a given distribution of relative humidity. *J. Atmos. Sci.*, **24**, 241–259, https://doi.org/10.1175/1520-0469(1967)024<0241:TEOTAW>2.0.CO;2.

Martínez-Castro, D., and Coauthors, 2019: The impact of microphysics parameterization in the simulation of two convective rainfall events over the Central Andres of Peru using WRF-ARW. *Atmosphere*, **10**, 442, https://doi.org/10.3390/atmos10080442.

Martynov, A., L. Sushama, and R. Laprise, 2010: Simulation of temperate freezing lakes by one-dimensional lake models: Performance assessment for interactive coupling with regional climate models. *Boreal Environ. Res.*, **15**, 143–164.

Mason, L. A., C. M. Riseng, A. D. Gronewold, E. S. Rutherford, J. Wang, A. Clites, S. D. P. Smith, and P. B. McIntyre, 2016: Fine-scale spatial variation in ice cover and surface temperature trends across the surface of the Laurentian Great Lakes. *Climatic Change*, **138**, 71–83, https://doi.org/10.1007/s10584-016-1721-2.

Mellor, G. L., and T. Yamada, 1982: Development of a turbulence closure model for geophysical fluid problems. *Rev. Geophys. Space Phys.*, **20**, 851–875, https://doi.org/10.1029/RG020i004p00851.

Mesinger, F., and Coauthors, 2006: North American regional reanalysis. *Bull. Amer. Meteor. Soc.*, **87**, 343–360, https://doi.org/10.1175/BAMS-87-3-343.

Mironov, D., 2008: Parameterization of lakes in numerical weather prediction: Description of a lake model. COSMO Tech. Rep. 11, 41 pp.

Mitchell, K., 2001: The Community Noah Land Surface Model Public Release Version 2.2 User's Guide. National Weather Service, National Center for Environmental Prediction, 26 pp., https://ral.ucar.edu/sites/default/files/public/product-tool/unified-noah-lsm/Noah_LSM_USERGUIDE_2.7.1.pdf.

Mlawer, E. J., S. J. Taubman, P. D. Brown, M. J. Iacono, and S. A. Clough, 1997: Radiative transfer for inhomogeneous atmospheres: RRTM, a validated correlated-k model for the longwave. *J. Geophys. Res.*, **102**, 16 663–16 682, https://doi.org/10.1029/97JD00237.

Mooney, P. A., F. J. Mulligan, and R. Fealy, 2013: Evaluation of the sensitivity of the Weather Research and Forecasting Model to parameterization schemes for regional climates of Europe

Brought to you by MIT LIBRARIES | Unauthenticated | Downloaded 09/22/21 12:14 PM UTC

over the period 1990-95. *J. Climate*, **26**, 1002–1017, https://doi.org/10.1175/JCLI-D-11-00676.1.

Morrison, H., G. Thompson, and V. Tatarskii, 2009: Impact of cloud microphysics on the development of training stratiform precipitation in a simulated squall line: Comparison of one and two-moment schemes. *Mon. Wea. Rev.*, **137**, 991–1007, https://doi.org/10.1175/2008MWR2556.1.

Moukomla, S., and P. D. Blanken, 2017: The estimation of the North American Great Lakes turbulent fluxes using satellite remote sensing and MERRA reanalysis data. *Remote Sens.*, **9**, 141, https://doi.org/10.3390/rs9020141.

Nakanish, M., 2001: Improvement of the Mellor-Yamada turbulence closure model based on large-eddy simulation data. *Bound.-Layer Meteor.*, **99**, 349–378, https://doi.org/10.1023/A:1018915827400.

Nakanishi, M., and H. Niino, 2006: An improved Mellor–Yamada level-3 model: Its numerical stability and application to a regional prediction of advection fog. *Bound.-Layer Meteor.*, **119**, 397–407, https://doi.org/10.1007/s10546-005-9030-8.

——, and ——, 2009: Development of an improved turbulence closure model for the atmospheric boundary layer. *J. Meteor. Soc. Japan*, **87**, 895–912, https://doi.org/10.2151/jmsj.87.895.

Nicholls, S. D., S. G. Decker, W.-K. Tao, S. E. Lang, J. J. Shi, and K. I. Mohr, 2017: Influence of bulk microphysics schemes upon Weather Research and Forecasting (WRF) version 3.6.1 nor'easter simulations. *Geosci. Model Dev.*, **10**, 1033–1049, https://doi.org/10.5194/gmd-10-1033-2017.

Niziol, T. A., 2003: An analysis of satellite-derived Great Lakes surface temperatures in regards to model simulations of lake effect snow. *10th Conf. on Mesoscale Processes*, Portland, OR, Amer. Meteor Soc., P1.9, https://ams.confex.com/ams/pdfpapers/63048.pdf.

——, W. R. Snyder, and J. S. Waldstreicher, 1995: Winter weather forecasting throughout the eastern United States. Part IV: Lake-effect snow. *Wea. Forecasting*, **10**, 61–77, https://doi.org/10.1175/1520-0434(1995)010<0061:WWFTTE>2.0.CO;2.

Notaro, M., K. Holman, A. Zarrin, E. Fluck, S. Vavrus, and V. Bennington, 2013a: Influence of the Laurentian Great Lakes on regional climate. *J. Climate*, **26**, 789–804, https://doi.org/10.1175/JCLI-D-12-00140.1.

——, A. Zarrin, S. Vavrus, and V. Bennington, 2013b: Simulation of heavy lake-effect snowstorms across the Great Lakes Basin by RegCM4: Synoptic climatology and variability. *Mon. Wea. Rev.*, **141**, 1990–2014, https://doi.org/10.1175/MWR-D-11-00369.1.

——, D. Lorenz, C. Hoving, and M. Schummer, 2014: Twenty-first century projections of snowfall and winter severity across central-eastern North America. *J. Climate*, **27**, 6526–6550, https://doi.org/10.1175/JCLI-D-13-00520.1.

——, V. Bennington, and S. Vavrus, 2015: Dynamically downscaled projections of lake-effect snow in the Great Lakes Basin. *J. Climate*, **28**, 1661–1684, https://doi.org/10.1175/JCLI-D-14-00467.1.

——, M. Schummer, Y. Zhong, S. Vavrus, L. Van Den Elsen, J. Coluccy, and C. Hoving, 2016: Projected influences of changes in weather severity on autumn-winter distributions of dabbling ducks in the Mississippi and Atlantic Flyways during the twenty-first century. *PLOS ONE*, **11**, e0167506, https://doi.org/10.1371/journal.pone.0167506.

Oleson, K. W., andCoauthors, 2013: Technical description of version 4.5 of the Community Land Model (CLM). NCAR Tech. Note NCAR/TN-503+STR, 420 pp., https://doi.org/10.5065/D6RR1W7M.

Orr, A., C. Listowski, M. Couttet, E. Collier, W. Immerzeel, P. Deb, and D. Bannister, 2017: Sensitivity of simulated summer monsoonal precipitation in Langtang Valley, Himalaya, to cloud microphysics schemes in WRF. *J. Geophys. Res. Atmos.*, **122**, 6298–6318, https://doi.org/10.1002/2016JD025801.

Otte, T. L., C. G. Nolte, M. J. Otte, and J. H. Bowden, 2012: Does nudging squelch the extremes in regional climate modeling? *J. Climate*, **25**, 7046–7066, https://doi.org/10.1175/JCLI-D-12-00048.1.

Oyler, J. W., A. Ballantyne, K. Jensco, M. Sweet, and S. W. Running, 2014: Creating a topoclimatic daily air temperature dataset for the conterminous United States using homogenized station data and remotely sensed land skin temperature. *Int. J. Climatol.*, **35**, 2258–2279, https://doi.org/10.1002/joc.4127.

Peltier, W. R., M. D'Orgeville, A. R. Erler, and F. Xie, 2018: Uncertainty in future summer precipitation in the Laurentian Great Lakes Basin: Dynamical downscaling and the influence of continental-scale processes on regional climate change. *J. Climate*, **31**, 2651–2673, https://doi.org/10.1175/JCLI-D-17-0416.1.

Peters-Lidard, C. D., and Coauthors, 2007: High-performance Earth system modeling with NASA/GSFC's Land Information System. *Innov. Syst. Software Eng.*, **3**, 157–165, https://doi.org/10.1007/s11334-007-0028-x.

——, and Coauthors, 2015: Integrated modeling of aerosol, cloud, precipitation and land processes at satellite resolved scales. *Environ. Modell. Software*, **67**, 149–159, https://doi.org/10.1016/j.envsoft.2015.01.007.

Petterssen, S., and P. A. Calabrese, 1959: On some weather influences due to warming of the air by the Great Lakes in winter. *J. Meteor.*, **16**, 646–652, https://doi.org/10.1175/1520-0469(1959)016<0646:OSWIDT>2.0.CO;2.

Pincus, R., H. W. Barker, and J.-J. Morcrette, 2003: A fast, flexible, approximate technique for computing radiative transfer in inhomogeneous cloud fields. *J. Geophys. Res.*, **108**, 4376, https://doi.org/10.1029/2002JD003322.

Pinker, R. T., and Coauthors, 2003: Surface radiation budgets in support of the GEWEX Continental-Scale International Project (GCIP) and the GEWEX Americas Prediction Project (GAPP), including the North American Land Data Assimilation System (NLDAS) project. *J. Geophys. Res.*, **108**, 8844, https://doi.org/10.1029/2002JD003301.

Pryor, S. C., D. Scavia, C. Downer, M. Gaden, L. Iverson, R. Nordstrom, J. Patz, and G. P. Robertson, 2014: Ch. 18: Midwest. *Climate Change Impacts in the United States: The Third National Climate Assessment*, J. M. Melillo, T. Richmond, and G. W. Yohe, Eds., U.S. Global Change Research Program, 418–440, https://nca2014.globalchange.gov/downloads/low/NCA3_Full_Report_18_Midwest_LowRes.pdf.

Qiu, B., and Coauthors, 2020: Implementation and evaluation of an improved lake scheme in Beijing Climate Center Atmosphere-Vegetation Interaction Model. *J. Geophys. Res. Atmos.*, **125**, e2019JD031272, https://doi.org/10.1029/2019JD031272.

Rockel, B., C. L. Castro, R. A. Pielke Sr., H. von Storch, and G. Leoncini, 2008: Dynamical downscaling: Assessment of model system dependent retained and added variability for two different regional climate models. *J. Geophys. Res.*, **113**, D05108, https://doi.org/10.1029/2007JD009461.

Rodriguez, Y., D. A. R. Kristovich, and M. R. Hjelmfelt, 2007: Lake-to-lake cloud bands: Frequencies and locations. *Mon. Wea. Rev.*, **135**, 4202–4213, https://doi.org/10.1175/2007MWR1960.1.

Brought to you by MIT LIBRARIES | Unauthenticated | Downloaded 09/22/21 12:14 PM UTC

Roeckner, E., and Coauthors, 2003: The atmospheric general circulation model ECHAM5: Part I: Model description. Tech. Rep. 349, 127 pp., https://mpimet.mpg.de/fileadmin/models/echam/mpi_report_349.pdf.

Samuelsson, P., E. Kourzeneva, and D. Mironov, 2010: The impact of lakes on the European climate as simulated by a regional climate model. *Boreal Environ. Res.*, **15**, 113–129.

Schoof, J., 2013: Historical and projected changes in human heat stress in the Midwestern United States. *Climate Change in The Midwest: Impacts, Risks, Vulnerability, and Adaptation*, S. C. Pryor, Ed., Indiana University Press, 146–157.

Schwab, D. J., G. Leshkevich, and G. Muhr, 1992: Satellite measurements of surface water temperature in the Great Lakes: Great Lakes Coastwatch. *J. Great Lakes Res.*, **18**, 247–258, https://doi.org/10.1016/S0380-1330(92)71292-1.

——, G. A. Leshkevich, and G. C. Muhr, 1999: Automated mapping of surface water temperature in the Great Lakes. *J. Great Lakes Res.*, **25**, 468–481, https://doi.org/10.1016/S0380-1330(99)70755-0.

Scott, R. W., and F. A. Huff, 1996: Impacts of Great Lakes on regional climate conditions. *J. Great Lakes Res.*, **22**, 845–863, https://doi.org/10.1016/S0380-1330(96)71006-7.

——, and ——, 1997: Lake effects on climate conditions in the Great Lakes basin. Illinois Water Survey MCC Research Rep. 97-01, 73 pp., https://www.isws.illinois.edu/pubdoc/CR/ISWSCR-617.pdf.

Sharma, A., and Coauthors, 2018: The need for an integrated land-lake-atmosphere modeling system, exemplified by North America's Great Lakes region. *Earth's Future*, **6**, 1366–1379, https://doi.org/10.1029/2018EF000870.

——, A. F. Hamlet, and H. J. S. Fernando, 2019: Lessons from inter-comparison of decadal climate simulations and observations for the Midwest U.S. and Great Lakes region. *Atmosphere*, **10**, 266, https://doi.org/10.3390/atmos10050266.

Shi, J. J., and Coauthors, 2010: WRF simulations of the 20-22 January 2007 snow events over eastern Canada: Comparison with in situ and satellite observations. *J. Appl. Meteor. Climatol.*, **49**, 2246–2266, https://doi.org/10.1175/2010JAMC2282.1.

Shi, Q., and P. Xue, 2019: Impact of lake surface temperature variations on lake effect snow over the Great Lakes region. *J. Geophys. Res. Atmos.*, **124**, 12 553–12 567, https://doi.org/10.1029/2019JD031261.

Skamarock, W. C., and Coauthors, 2008: A description of the Advanced Research WRF version 3. NCAR Tech. Note NCAR/TN-475+STR, 113 pp., https://doi.org/10.5065/D68S4MVH.

Spence, C., P. D. Blanken, N. Hedstrom, V. Fortin, and H. Wilson, 2011: Evaporation from Lake Superior: 2. Spatial distribution and variability. *J. Great Lakes Res.*, **37**, 717–724, https://doi.org/10.1016/j.jglr.2011.08.013.

——, ——, J. D. Lenters, and N. Hedstrom, 2013: The importance of spring and autumn atmospheric conditions for the evaporation regime of Lake Superior. *J. Hydrometeor.*, **14**, 1647–1658, https://doi.org/10.1175/JHM-D-12-0170.1.

——, N. Hedstrom, P. D. Blanken, J. Lenters, and G. J. Cutrell, 2019: Great Lakes Evaporation Network (GLEN) data. Great Lakes Observing System (GLOS), http://tds.glos.us/thredds/catalog/glos/glen/catalog.html.

Spero, T. L., M. J. Otte, J. H. Bowden, and C. G. Nolte, 2014: Improving the representation of clouds, radiation, and precipitation using spectral nudging in the Weather Research and Forecasting model. *J. Geophys. Res. Atmos.*, **119**, 11 682–11 694, https://doi.org/10.1002/2014JD022173.

——, C. G. Nolte, J. H. Bowden, M. S. Mallard, and J. A. Herwehe, 2016: The impact of incongruous lake temperatures on regional climate extremes downscaled from the CMIP5 archive using the WRF Model. *J. Climate*, **29**, 839–853, https://doi.org/10.1175/JCLI-D-15-0233.1.

Stepanenko, V. M., S. Goyette, A. Martynov, M. Perroud, X. Fang, and D. Mironov, 2010: First steps of a Lake Model Intercomparison Project: LakeMIP. *Boreal Environ. Res.*, **15**, 191–202.

Subin, Z. M., W. J. Riley, and D. V. Mironov, 2012: An improved lake model for climate simulations: Model structure, evaluation, and sensitivity analyses in CESM1. *J. Adv. Model. Earth Syst.*, **4**, M02001, https://doi.org/10.1029/2011MS000072.

Suriano, Z. J., and D. J. Leathers, 2017: Synoptically classified lake-effect snowfall trends to the lee of Lakes Erie and Ontario. *Climate Res.*, **74**, 1–13, https://doi.org/10.3354/cr01480.

Tang, J., S. Wang, X. Niu, P. Hui, P. Zong, and X. Wang, 2017: Impact of spectral nudging on regional climate simulation over CORDEX East Asia using WRF. *Climate Dyn.*, **48**, 2339–2357, https://doi.org/10.1007/s00382-016-3208-2.

Tao, W.-K., J. Simpson, and M. McCumber, 1989: An ice-water saturation adjustment. *Mon. Wea. Rev.*, **117**, 231–235, https://doi.org/10.1175/1520-0493(1989)117<0231:AIWSA>2.0.CO;2.

Thompson, G., P. R. Field, R. M. Rasmussen, and W. D. Hall, 2008: Explicit forecasts of winter precipitation using an improved bulk microphysics scheme. Part II: Implementation of a new snow parameterization. *Mon. Wea. Rev.*, **136**, 5095–5115, https://doi.org/10.1175/2008MWR2387.1.

Thornton, P. E., S. W. Running, and M. A. White, 1997: Generating surfaces of daily meteorology variables over large regions of complex terrain. *J. Hydrol.*, **190**, 214–251, https://doi.org/10.1016/S0022-1694(96)03128-9.

——, M. M. Thornton, B. W. Mayer, N. Wilhelmi, Y. Wei, R. Devarakonda, and R. B. Cook, 2014: Daymet: Daily surface weather on a 1-km grid for North America, version 2. Oak Ridge National Laboratory Distributed Active Archive Center, accessed 15 November 2014, https://doi.org/10.3334/ORNLDAAC/1219.

Tiedtke, M., 1989: A comprehensive mass flux scheme for cumulus parameterization in large-scale models. *Mon. Wea. Rev.*, **117**, 1779–1800, https://doi.org/10.1175/1520-0493(1989)117<1779:ACMFSF>2.0.CO;2.

Todorovich, P., 2009: America's emerging megaregions and implications for a national growth strategy. *Int. J. Public Sector Manage.*, **22**, 221–234, https://doi.org/10.1108/09513550910949208.

Vaccaro, L., and J. Read, 2011: Vital to our nation's economy: Great Lakes jobs. Michigan Sea Grant 2011 Rep., 7 pp., http://www.fws.gov/glri/documents/2011GreatLakesJobsReport.pdf.

Van Cleave, K., J. D. Lenters, J. Wang, and E. M. Verhamme, 2014: A regime shift in Lake Superior ice cover, evaporation, and water temperature following the warm El Nino winter of 1997-1998. *Limnol. Oceanogr.*, **59**, 1889–1898, https://doi.org/10.4319/lo.2014.59.6.1889.

Wang, J., and V. R. Kotamarthi, 2013: Assessment of dynamical downscaling in near-surface fields with different spectral nudging approaches using the Nested Regional Climate Model (NRCM). *J. Appl. Meteor. Climatol.*, **52**, 1576–1591, https://doi.org/10.1175/JAMC-D-12-0302.1.

——, H. Hu, D. Schwab, G. Leshkevich, D. Beletsky, N. Hawley, and A. Clites, 2010: Development of the Great Lakes Ice-circulation Model (GLIM): Application to Lake Erie in 2003–2004. *J. Great Lakes Res.*, **36**, 425–436, https://doi.org/10.1016/j.jglr.2010.04.002.

Brought to you by MIT LIBRARIES | Unauthenticated | Downloaded 09/22/21 12:14 PM UTC

——, X. Bai, H. Hu, A. Clites, M. Colton, and B. Lofgren, 2012: Temporal and spatial variability of Great Lakes ice cover, 1973–2010. *J. Climate*, **25**, 1318–1329, https://doi.org/10.1175/2011JCLI4066.1.

Weston, M., N. Chaouch, V. Valappil, M. Temimi, M. Ek, and W. Zheng, 2019: Assessment of the sensitivity to the thermal roughness length in Noah and Noah-MP Land Surface Model using WRF in an arid region. *Pure Appl. Geophys.*, **176**, 2121–2137, https://doi.org/10.1007/s00024-018-1901-2.

Winkler, J. A., R. W. Arritt, and S. C. Pryor, 2012: Climate projections for the Midwest: Availability, interpretation and synthesis. US National Climate Assessment Midwest Tech. Input Rep., 24 pp., http://glisa.umich.edu/media/files/NCA/MTIT_Future.pdf.

Wright, D. M., D. J. Posselt, and A. L. Steiner, 2013: Sensitivity of lake-effect snowfall to lake ice cover and temperature in the Great Lakes region. *Mon. Wea. Rev.*, **141**, 670–689, https://doi.org/10.1175/MWR-D-12-00038.1.

Wu, D., C. Peters-Lidard, W.-K. Tao, and W. Peterson, 2016: Evaluation of NU-WRF rainfall forecasts for IFloodS. *J. Hydrometeor.*, **17**, 1317–1335, https://doi.org/10.1175/JHM-D-15-0134.1.

Wuebbles, D. J., and K. Hayhoe, 2004: Climate change projections for the United States Midwest. *Mitigation Adapt. Strategies Global Change*, **9**, 335–363, https://doi.org/10.1023/B:MITI.0000038843.73424.de.

——, ——, and J. Parzen, 2010: Introduction: Assessing the effects of climate change on Chicago and the Great Lakes. *J. Great Lakes Res.*, **36**, 1–6, https://doi.org/10.1016/j.jglr.2009.09.009.

Xia, Y., and Coauthors, 2012: Continental-scale water and energy flux analysis and validation for North American Land Data Assimilation System project phase 2 (NLDAS-2): 2. Validation of model-simulated streamflow. *J. Geophys. Res.*, **117**, D03110, https://doi.org/10.1029/2011JD016051.

Xiao, C., B. M. Lofgren, J. Wang, and P. Y. Chu, 2016: Improving the lake scheme within a coupled WRF-lake model in the Laurentian Great Lakes. *J. Adv. Model. Earth Syst.*, **8**, 1969–1985, https://doi.org/10.1002/2016MS000717.

——, ——, and ——, 2018: WRF-based assessment of the Great Lakes' impact on cold season synoptic cyclones. *Atmos. Res.*, **214**, 189–203, https://doi.org/10.1016/j.atmosres.2018.07.020.

Xu, X., S. K. Frey, A. Boluwade, A. R. Erler, O. Khader, D. R. Lapen, and E. Sudicky, 2019: Evaluation of variability among different precipitation products in the Northern Great Plains. *J. Hydrol. Reg. Stud.*, **24**, 100608, https://doi.org/10.1016/j.ejrh.2019.100608.

Xue, P., D. J. Schwab, and S. Hu, 2015: An investigation of the thermal response to meteorological forcing in a hydrodynamic model of Lake Superior. *J. Geophys. Res. Oceans*, **120**, 5233–5253, https://doi.org/10.1002/2015JC010740.

——, J. S. Pal, X. Ye, J. D. Lenters, C. Huang, and P. Y. Chu, 2017: Improving the simulation of large lakes in regional climate modeling: Two-way lake–atmosphere coupling with a 3D hydrodynamic model of the Great Lakes. *J. Climate*, **30**, 1605–1627, https://doi.org/10.1175/JCLI-D-16-0225.1.

Yang, T.-Y., J. Kessler, L. Mason, P. Y. Chu, and J. Wang, 2020: A consistent Great Lakes ice cover digital data set for winters 1973-2019. *Sci. Data*, **7**, 259, https://doi.org/10.1038/s41597-020-00603-1.

Ye, X., E. J. Anderson, P. Y. Chu, C. Huang, and P. Xue, 2019: Impact of water mixing and ice formation on the warming of Lake Superior: A model-guided mechanism study. *Limnol. Oceanogr.*, **64**, 558–574, https://doi.org/10.1002/lno.11059.

Zahmatkesh, Z., D. Tapsoba, J. Leach, and P. Coulibaly, 2019: Evaluation and bias correction of SNODAS snow water equivalent (SWE) for streamflow simulation in eastern Canadian basins. *Hydrol. Sci. J.*, **64**, 1541–1555, https://doi.org/10.1080/02626667.2019.1660780.

Zhang, C., Y. Wang, and K. Hamilton, 2011: Improved representation of boundary layer clouds over the southeast Pacific in ARW–WRF using a modified Tiedtke cumulus parameterization scheme. *Mon. Wea. Rev.*, **139**, 3489–3513, https://doi.org/10.1175/MWR-D-10-05091.1.

Zhang, D.-L., and R. A. Anthes, 1982: A high-resolution model of the planetary boundary layer—Sensitivity tests and comparisons with SESAME-79 data. *J. Appl. Meteor.*, **21**, 1594–1609, https://doi.org/10.1175/1520-0450(1982)021<1594:AHRMOT>2.0.CO;2.

Zhang, L., Y. Zhao, D. Hein-Griggs, T. Janes, S. Tucker, and J. J. H. Ciborowski, 2020: Climate change projections of temperature and precipitation for the Great Lakes Basin using the PRECIS regional climate model. *J. Great Lakes Res.*, **46**, 255–266, https://doi.org/10.1016/j.jglr.2020.01.013.

Zhong, S., X. Li, X. Bian, W. E. Heilman, L. R. Leung, and W. I. Gustafson Jr., 2012: Evaluation of regional climate simulations over the Great Lakes region driven by three global data sets. *J. Great Lakes Res.*, **38**, 212–225, https://doi.org/10.1016/j.jglr.2012.03.012.

Zhong, Y., M. Notaro, S. J. Vavrus, and M. J. Foster, 2016: Recent accelerated warming of the Laurentian Great Lakes: Physical drivers. *Limnol. Oceanogr.*, **61**, 1762–1786, https://doi.org/10.1002/lno.10331.

Zobel, Z., J. Wang, D. J. Wuebbles, and V. R. Kotamarthi, 2017: High-resolution dynamical downscaling ensemble projections of future extreme temperature distributions for the United States. *Earth's Future*, **5**, 1234–1251, https://doi.org/10.1002/2017EF000642.

——, ——, ——, and ——, 2018: Analyses for high-resolution projections through the end of the 21st century for precipitation extremes over the United States. *Earth's Future*, **6**, 1471–1490, https://doi.org/10.1029/2018EF000956.

Brought to you by MIT LIBRARIES | Unauthenticated | Downloaded 09/22/21 12:14 PM UTC